

Comprehensive study of the light charged Higgs boson in the type-I two-Higgs-doublet model

Kingman Cheung,^{1,2,3,*} Adil Jueid,^{4,1,†} Jinheung Kim,^{1,‡}

Soojin Lee,^{1,§} Chih-Ting Lu,^{5,¶} and Jeonghyeon Song^{1,**}

¹*Department of Physics, Konkuk University, Seoul 05029, Republic of Korea*

²*Department of Physics, National Tsing Hua University, Hsinchu 300, Taiwan*

³*Center for Theory and Computation,*

National Tsing Hua University, Hsinchu 300, Taiwan

⁴*Quantum Universe Center, Korea Institute for*

Advanced Study, Seoul 02455, Republic of Korea

⁵*School of Physics, Korea Institute for Advanced Study, Seoul 02455, Republic of Korea*

Abstract

In the type-I two-Higgs-doublet model, existing theoretical and experimental constraints still permit the light charged Higgs boson with a mass below the top quark mass. We present a complete roadmap for the light charged Higgs boson at the LHC through the comprehensive phenomenology study. In type-I, it is challenging to simultaneously accommodate the light mass of the charged Higgs boson and the constraints from theory, electroweak precision data, Higgs data, $b \rightarrow s\gamma$, and direct search bounds. Consequently, the extremely curtailed parameter space predicts quite definite phenomenological implications. We point out that the mass of the pseudoscalar Higgs boson, M_A , is the most crucial factor. If M_A is light, the charged Higgs boson decays mainly into AW^\pm . When M_A is above the AW^\pm threshold, on the other hand, the dominant decay mode is into $\tau^\pm\nu$. Over the whole viable parameter space, we study all the possible production and decay modes of charged Higgs bosons at the LHC, and suggest three efficient channels: (i) $pp \rightarrow H^+H^- \rightarrow [\tau\nu][\tau\nu]$; (ii) $pp \rightarrow HA/HH/AA \rightarrow H^\pm W^\mp H^\pm W^\mp \rightarrow [\tau\nu][\tau\nu]WW$; (iii) $pp \rightarrow H^+H^- \rightarrow [b\bar{b}W][b\bar{b}W]$. Based on the sophisticated signal-background analyses including detector simulation, we showed that the significance of the first final state is large, that of the second one is marginal around three, but the third one suffers from huge $t\bar{t}$ related backgrounds.

Keywords: Higgs Physics, Beyond the Standard Model

*Electronic address: cheung@phys.nthu.edu.tw

†Electronic address: adiljueid@kias.re.kr

‡Electronic address: jinheung.kim1216@gmail.com

§Electronic address: soojinlee957@gmail.com

¶Electronic address: timluyu@gmail.com

**Electronic address: jhsong@konkuk.ac.kr

Contents

I. Introduction	2
II. Review of type-I 2HDM	5
III. Characteristics of type-I with light charged Higgs bosons	6
A. Theoretical and experimental constraints	6
B. Characteristics of surviving parameters	8
IV. Production of light charged Higgs bosons at the LHC	12
V. Signal-background analysis for $[bbW][bbW]$, $[\tau\nu][\tau\nu]$, and $[\tau\nu][\tau\nu]WW$	15
A. $[\tau\nu][\tau\nu]$	17
B. $[\tau^\pm\nu][\tau^\pm\nu]W^\mp W^\mp$	20
C. $[bbW][bbW]$	23
VI. Conclusions	26
Acknowledgments	27
References	28

I. INTRODUCTION

The discovery of the Higgs boson at the LHC in 2012 [1, 2] is a triumph achieved through cooperation between the theoretical and experimental communities in particle physics. Despite the completion of the standard model (SM), however, we still long for the next milestone to progress toward the final theory of the Universe, as facing the baffling questions such as the naturalness problem, the fermion mass hierarchy, the origin of CP violation in the quark sector, the baryogenesis, the non-zero neutrino masses, and the identity of dark matter. Since 2012, the ATLAS and CMS collaborations have searched hard for the same success as the observed Higgs boson, a dramatic resonance bump in invariant mass distribution, but not achieved any success so far. A new direction of research arises in the framework of the SM effective field theory [3] where we systematically characterize the experimental deviations from the SM predictions without specifying the UV physics.

Nevertheless, direct searches for new particles should continue because they can explicitly reveal an essential aspect of the new physics (NP) theory. Many NP models have an extended Higgs sector. When additional Higgs doublets, triplets, or higher representations are included, a distinguished new particle is the charged Higgs boson H^\pm . If H^\pm is light at a mass below the top quark mass, the implication on the UV theory shall be further profound. From this perspective, we consider the light charged Higgs boson in the two-Higgs-doublet model (2HDM) [4, 5], which

Decay Production	$[\tau^\pm \nu]$	$[cb]$	$[cs]$	$[W^\pm \varphi^0/A]$	$[W^\pm h_{\text{SM}}/A]$
$t \rightarrow H^\pm b$	type-I [9] type-X [13]	3HDM [10]	3HDM [10]	IS type-I [11] N2HDM [14]	type-I [12]
	ATLAS [7] CMS [8]	ATLAS [15] CMS [18]	ATLAS [16] CMS [19, 20]	CMS [17]	
$W^{\pm*} \rightarrow H^\pm \varphi^0$				IS type-I [21]	
$W^{\pm*} \rightarrow H^\pm A$	type-X [22]			IS type-I,X [23, 24]	
$pp \rightarrow H^+ H^-$				IS type-I,X [23, 24]	
$qb \rightarrow q' b H^\pm$	MSSM [25]				
$cs/cb \rightarrow H^\pm$	type-III [26, 27]				
$W^{\pm*} W^{\pm*} \rightarrow H^\pm H^\pm$	$\mathcal{B}_{\tau\nu} = 1$ [28]			type-I,X [29]	

Table I: Theoretical and experimental studies on a light charged Higgs boson in the 2HDM and 3HDM at the LHC, classified according to the production and decay channels. φ^0 denotes a CP -even scalar boson with a mass below 125 GeV. The theoretical model is also presented: type-I, type-X, and type-III denote the type of 2HDM, “IS” denotes the inverted scenario for $h_{\text{SM}} = H$ in the 2HDM, and 3HDM is the three-Higgs-doublet model.

accommodates five Higgs bosons, CP -even neutral h and H ($m_h < M_H$), CP -odd neutral A , and a pair of charged H^\pm . The charged Higgs boson in type-II and type-Y is tightly constrained to be as heavy as $M_{H^\pm} \gtrsim 580$ GeV due to the measurements of the inclusive weak radiative B -meson decay into $s\gamma$ [6]. Only type-I and type-X can accommodate a light H^\pm . We concentrate on type-I in this paper. In type-I, all the Yukawa couplings of H^\pm are inversely proportional to $\tan\beta$, the ratio of two vacuum expectation values of two Higgs-doublet fields. The decay branching ratios of H^\pm into a fermion pair are proportional to the fermion mass, which suggested the main search mode at the LHC as the production via the decay of the top quark $t \rightarrow bH^+$, followed by the decay $H^\pm \rightarrow \tau\nu$. Both the ATLAS and CMS collaborations have analyzed this mode [7, 8], presenting the upper bound on $\mathcal{B}(t \rightarrow bH^\pm) \times \mathcal{B}(H^\pm \rightarrow \tau\nu)$. The absence of new signal demands large $\tan\beta$, e.g., $\tan\beta \gtrsim 10$ for $M_{H^\pm} = 110$ GeV, which highly suppresses $\mathcal{B}(t \rightarrow bH^\pm)$ below $\mathcal{O}(10^{-4})$. Thereupon we come to question whether $t \rightarrow bH^\pm$ is indeed the golden mode for the light charged Higgs boson in type-I.

In this regard, other production and decay channels of the light charged Higgs boson in the 2HDM and 3HDM at the LHC¹ have been studied recently. We summarize the literature survey

¹ Future colliders have been shown efficient for production of a light H^\pm , such as future electron-proton colliders for H^\pm in type-III 2HDM [30] and three-Higgs-doublet model [10, 31].

on the light charged Higgs boson² in Table I, specifying the theoretical model³, the production channel, and the decay mode. Here “IS” stands for the inverted scenario where the observed Higgs boson at a mass of 125 GeV is the heavier CP -even H , while the light CP -even Higgs boson, denoted by φ^0 in Table I, has not been observed yet [11, 21, 23, 24, 37–39]. The studies in Table I reveal some aspects of the characteristics of the light charged Higgs boson in type-I, but not the whole, because they focus on one or two specific channels. In addition, many studies are based on some conditions such as the Higgs alignment limit for the SM-like Higgs boson [38, 40–44] and the mass degeneracy of new Higgs bosons for the electroweak precision data [38, 45, 46]. But the conditions could have interfered with the observation at the LHC. In order not to miss the light charged Higgs boson, therefore, we need a full roadmap over the whole viable parameter space of type-I. Then, it is essential to investigate all the possible production and decay modes as well as the optimal and representative channel for each region of the parameter space.

To achieve the goal, we will explore the entire parameter space of type-I with the light H^\pm , and obtain the phenomenologically viable parameters. As shall be shown, imposing light M_{H^\pm} restricts the model severely. In turn, the model parameters are strongly correlated with each other, and the signal rates of light charged Higgs bosons at the LHC have quite definite values throughout the allowed parameter space. Based on these results, we will suggest three channels to cover the whole parameter space effectively: (i) $pp \rightarrow H^+H^- \rightarrow [\tau\nu][\tau\nu]$; (ii) $pp \rightarrow HA/HH/AA \rightarrow H^\pm W^\mp H^\pm W^\mp \rightarrow [\tau\nu][\tau\nu]WW$; (iii) $pp \rightarrow H^+H^- \rightarrow [b\bar{b}W][b\bar{b}W]$. Using sophisticated signal-background analysis techniques with the detector simulation, the LHC discovery potentials of the proposed channels are to be rigorously obtained. These are our new contributions.

The paper is organized as follows. In Sec. II, we briefly review the type-I 2HDM with CP invariance and softly broken Z_2 parity. In Sec. III, we present the results of random scans by placing the theoretical and experimental constraints for $M_{H^\pm} = 110, 140$ GeV. The characteristic features of the allowed parameters are to be discussed, including the branching ratios of the new Higgs bosons. Section IV deals with the production channels of a light H^\pm at the LHC. After finding all the possible signals, we suggest three main processes which can cover the allowed parameter space. In Sec. V, we perform the signal-to-background analysis for $pp \rightarrow [\tau\nu][\tau\nu]$, $pp \rightarrow [\tau\nu][\tau\nu]WW$, and $pp \rightarrow [b\bar{b}W][b\bar{b}W]$ at the HL-LHC. Conclusions are given in Sec. VI.

² Some unconventional decay channels of the heavy H^\pm in the 2HDM have also been studied, such as $H^\pm \rightarrow W^\pm A$ [32], $H^\pm \rightarrow W^\pm \gamma$ [33], and $H^\pm \rightarrow t\bar{b}$ [34–36].

³ In Ref. [28], $\mathcal{B}_{\tau\nu} \equiv \mathcal{B}(H^\pm \rightarrow \tau^\pm \nu) = 1$ is assumed without specifying the type of the 2HDM.

II. REVIEW OF TYPE-I 2HDM

The 2HDM accommodates two complex $SU(2)_L$ Higgs doublet scalar fields, Φ_1 and Φ_2 [4]:

$$\Phi_i = \begin{pmatrix} w_i^+ \\ \frac{v_i + h_i + i\eta_i}{\sqrt{2}} \end{pmatrix}, \quad i = 1, 2, \quad (1)$$

where v_1 and v_2 are the nonzero vacuum expectation values of Φ_1 and Φ_2 , respectively. The ratio of v_2 to v_1 defines the mixing angle β by $\tan \beta = v_2/v_1$. In what follows, we use the simplified notation of $s_x = \sin x$, $c_x = \cos x$, and $t_x = \tan x$. The electroweak symmetry is broken by $v = \sqrt{v_1^2 + v_2^2} = 246$ GeV. The flavor-changing-neutral-current (FCNC) at tree level is prevented by a discrete Z_2 symmetry, under which $\Phi_1 \rightarrow \Phi_1$ and $\Phi_2 \rightarrow -\Phi_2$ [47, 48]. Then the most general and renormalizable scalar potential with CP invariance is

$$\begin{aligned} V = & m_{11}^2 \Phi_1^\dagger \Phi_1 + m_{22}^2 \Phi_2^\dagger \Phi_2 - m_{12}^2 (\Phi_1^\dagger \Phi_2 + \text{H.c.}) \\ & + \frac{1}{2} \lambda_1 (\Phi_1^\dagger \Phi_1)^2 + \frac{1}{2} \lambda_2 (\Phi_2^\dagger \Phi_2)^2 + \lambda_3 (\Phi_1^\dagger \Phi_1) (\Phi_2^\dagger \Phi_2) + \lambda_4 (\Phi_1^\dagger \Phi_2) (\Phi_2^\dagger \Phi_1) \\ & + \frac{1}{2} \lambda_5 [(\Phi_1^\dagger \Phi_2)^2 + \text{H.c.}], \end{aligned} \quad (2)$$

where the m_{12}^2 term softly breaks the Z_2 parity. The model accommodates five physical Higgs bosons, the light CP -even scalar h , the heavy CP -even scalar H , the CP -odd pseudoscalar A , and a pair of charged Higgs bosons H^\pm . The relations of the physical Higgs bosons with the weak eigenstates in Eq. (1) via two mixing angles α and β are referred to Ref. [33].

The SM Higgs boson h_{SM} is

$$h_{\text{SM}} = s_{\beta-\alpha} h + c_{\beta-\alpha} H. \quad (3)$$

We take the normal scenario where the observed Higgs boson is h . Of special importance is the Higgs alignment limit where $h = h_{\text{SM}}$. When $s_{\beta-\alpha} = 1$, $H \rightarrow WW/ZZ$, $A \rightarrow Zh$, and $H^\pm \rightarrow W^{\pm(*)}h$ are prohibited at tree level, but the exotic Higgs decay $h \rightarrow AA$ is allowed if A is light enough. In this paper, we do not make any assumption on the model parameters and let the theoretical and experimental constraints determine the phenomenology.

We take the physical parameter basis of

$$\{m_h, \quad M_{H^\pm}, \quad M_H, \quad M_A, \quad m_{12}^2, \quad t_\beta, \quad s_{\beta-\alpha}\}, \quad (4)$$

where $\beta - \alpha \in [0, \pi]$.⁴ The quartic couplings in the scalar potential play an essential role in

⁴ The public codes such as 2HDMC [49], HIGGSIGNALS [50], and HIGGSBOUNDS [51] take the range of $(\beta - \alpha) \in [-\pi/2, \pi/2]$, but most of the theoretical studies adopt the convention of $s_{\beta-\alpha} > 0$. For the immediate comparison with other theoretical studies, we present the results in the positive $s_{\beta-\alpha}$ scheme: if $s_{\beta-\alpha}^{2\text{HDMC}} < 0$, $(\beta - \alpha) = (\beta - \alpha)^{2\text{HDMC}} + \pi$.

satisfying the theoretical constraints. In terms of the model parameters, they are given as [45]

$$\begin{aligned}
\lambda_1 &= \frac{1}{v^2} [m_h^2 (s_{\beta-\alpha} - c_{\beta-\alpha} t_\beta)^2 + M_H^2 (s_{\beta-\alpha} t_\beta + c_{\beta-\alpha})^2 - M^2 t_\beta^2], \\
\lambda_2 &= \frac{1}{v^2} \left[m_h^2 \left(s_{\beta-\alpha} + \frac{c_{\beta-\alpha}}{t_\beta} \right)^2 - \frac{M^2}{t_\beta^2} + M_H^2 \left(\frac{s_{\beta-\alpha}}{t_\beta} - c_{\beta-\alpha} \right)^2 \right], \\
\lambda_3 &= \frac{1}{v^2} \left[(m_h^2 - M_H^2) \left\{ s_{\beta-\alpha}^2 - s_{\beta-\alpha} c_{\beta-\alpha} \left(t_\beta - \frac{1}{t_\beta} \right) - c_{\beta-\alpha}^2 \right\} + 2M_{H^\pm}^2 - M^2 \right], \\
\lambda_4 &= \frac{1}{v^2} [M^2 + M_A^2 - 2M_{H^\pm}^2], \\
\lambda_5 &= \frac{1}{v^2} [M^2 - M_A^2],
\end{aligned} \tag{5}$$

where $M^2 = m_{12}^2 / (s_\beta c_\beta)$.

The gauge couplings of the Higgs bosons are described by

$$\begin{aligned}
\mathcal{L}_{\text{gauge}} &= \left(gm_W W_\mu^\dagger W^\mu + \frac{1}{2} g_Z m_Z Z_\mu Z^\mu \right) (s_{\beta-\alpha} h + c_{\beta-\alpha} H) \\
&+ \frac{g}{2} i \left[W_\mu^+ (c_{\beta-\alpha} h - s_{\beta-\alpha} H) \overleftrightarrow{\partial}^\mu H^- - H.c. \right] - \frac{g}{2} \left[W_\mu^+ H^- \overleftrightarrow{\partial}^\mu A + H.c. \right] \\
&+ i \left\{ e A_\mu + \frac{g_Z}{2} (s_W^2 - c_W^2) Z_\mu \right\} H^+ \overleftrightarrow{\partial}^\mu H^- + \frac{g_Z}{2} Z_\mu \left[c_{\beta-\alpha} A \overleftrightarrow{\partial}^\mu h - s_{\beta-\alpha} A \overleftrightarrow{\partial}^\mu H \right],
\end{aligned} \tag{6}$$

where $s_W = \sin \theta_W$, $g_Z = g/c_W$, and $f \overleftrightarrow{\partial}^\mu g \equiv (f \partial^\mu g - g \partial^\mu f)$. The Yukawa couplings to the SM fermions are defined by

$$\begin{aligned}
\mathcal{L}_{\text{Yuk}} &= - \sum_f \left(\frac{m_f}{v} \kappa_f \bar{f} f h + \frac{m_f}{v} \xi_f^H \bar{f} f H - i \frac{m_f}{v} \xi_f^A \bar{f} \gamma_5 f A \right) \\
&- \left\{ \frac{\sqrt{2} V_{ud}}{v} H^+ \bar{u} (m_u \xi_u^A P_L + m_d \xi_d^A P_R) d + \frac{\sqrt{2} m_\tau}{v} H^+ \xi_\tau^A \bar{\nu}_L \tau_R + \text{H.c.} \right\},
\end{aligned} \tag{7}$$

where κ_f and $\xi_f^{H,A}$ in type-I are

$$\kappa_f = s_{\beta-\alpha} + \frac{c_{\beta-\alpha}}{t_\beta}, \quad \xi_f^H = -\frac{s_{\beta-\alpha}}{t_\beta} + c_{\beta-\alpha}, \quad \xi_u^A = -\xi_d^A = -\xi_\tau^A = \frac{1}{t_\beta}. \tag{8}$$

III. CHARACTERISTICS OF TYPE-I WITH LIGHT CHARGED HIGGS BOSONS

A. Theoretical and experimental constraints

We study the implication of the theoretical and experimental constraints on type-I with a light H^\pm . Two cases for M_{H^\pm} are considered:

$$M_{H^\pm} = 110, 140 \text{ GeV}. \tag{9}$$

The other parameters are scanned over the following ranges:

$$\begin{aligned} t_\beta &\in [1.7, 50], \quad s_{\beta-\alpha} \in [0.75, 1], \\ M_H &\in [130, 3000] \text{ GeV}, \quad M_A \in [15, 3000] \text{ GeV}, \quad m_{12}^2 \in [-3000^2, 3000^2] \text{ GeV}^2. \end{aligned} \quad (10)$$

The condition of $t_\beta > 1.7$ makes type-I consistent with the observation of $b \rightarrow s\gamma$ [6]. The range of $s_{\beta-\alpha}$ is from the current Higgs precision data [52]. For M_H , we avoid the case where M_H is too close to the observed Higgs boson mass.

With the prepared random parameter sets, we impose the following constraints:

Step-(i) Theory+EWPD+FCNC: We require the parameter set to satisfy the conditions in three categories.

- Theoretical constraints

1. Higgs potential being bounded from below [53];
2. Perturbative unitarity of the amplitudes of scalar-scalar, scalar-vector, and vector-vector scatterings at high energies [54, 55];
3. Perturbativity of the quartic couplings [4, 38];
4. Vacuum stability [56].

The detailed expressions are referred to the references.

- Electroweak precision data

We calculate the Peskin-Takeuchi electroweak oblique parameters in the 2HDM [57–59] and require $\chi^2 < 7.815$ for the current best-fit results of [59]

$$S = -0.01 \pm 0.10, \quad T = 0.03 \pm 0.12, \quad U = 0.02 \pm 0.11, \quad (11)$$

where the correlations among the oblique parameters have been properly taken into account.

- $b \rightarrow s\gamma$ constraints

We consider the most sensitive FCNC process to the 2HDM, $b \rightarrow s\gamma$ [6].

Step-(ii) Higgs precision data: To check the consistency with the Higgs precision data, we use HIGGSIGNALS-v2.2.0 [50], which yields the χ^2 output for 107 Higgs observables [60–67]. Since there are five model parameters with the given M_{H^\pm} , the number of degrees of freedom is 102. We demand that the p -value be larger than 0.05. In addition, the total width of the Higgs boson is required to be within the experimental upper bound at 95% C.L., i.e., $\Gamma_h^{\text{tot}} < 9.16 \text{ MeV}$ [68].

Step-(iii) Direct searches: Using HIGGSBOUNDS-5 [51], we calculate $r_{95\%}$ for each direct search process at the LEP, Tevatron, and LHC, defined by

$$r_{95\%} = \frac{S_{\text{type-I}}}{S_{\text{obs}}^{95\%}}, \quad (12)$$

where $S_{\text{type-I}}$ is the predicted cross section in the model and $S_{\text{obs}}^{95\%}$ is the observed upper bound on the cross section at the 95% C.L. A parameter set is excluded if $r_{95\%} > 1$.

B. Characteristics of surviving parameters

We perform the random scan over the full five-dimensional parameter space and cumulatively impose the constraints in Step-(i), Step-(ii), and Step-(iii). First, we obtained 10^6 parameter sets that satisfy Step-(i) for $M_{H^\pm} = 110$ GeV and another 10^6 for $M_{H^\pm} = 140$ GeV. After applying the constraints at Step-(ii), about 24.4% (27.4%) of 10^6 parameter sets survive for $M_{H^\pm} = 110$ (140) GeV. Step-(iii) is most powerful in restricting the model: only 0.22% (1.1%) of the parameter sets after Step-(i) are allowed for $M_{H^\pm} = 110$ (140) GeV. The smoking-gun process is the LHC search for $pp \rightarrow t\bar{t}$ followed by $t \rightarrow H^+b \rightarrow \tau\nu + b$ [7], which excludes more than 99% of the parameter sets that passed Step-(ii).

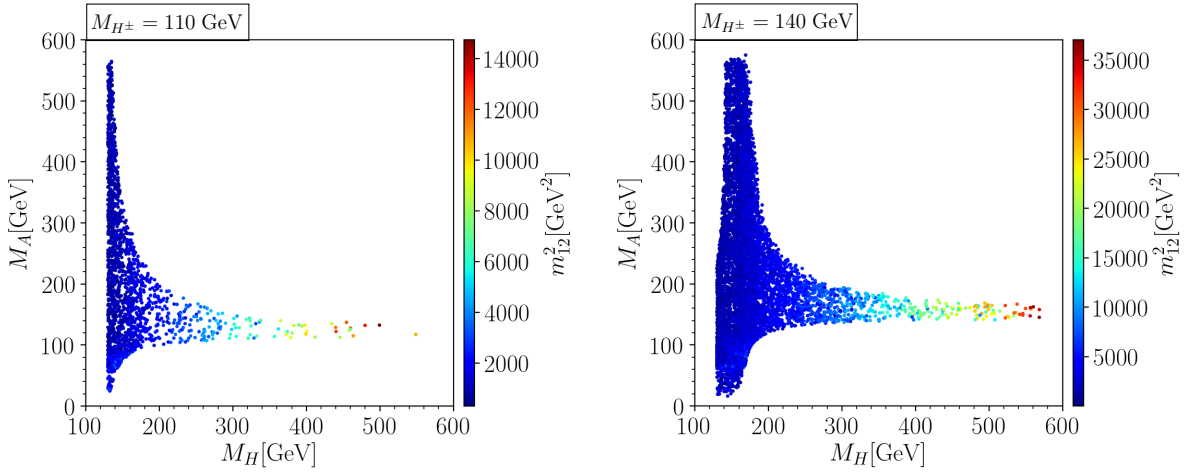


Figure 1: M_A vs M_H with the color code indicating the value of m_{12}^2 . We fix $M_{H^\pm} = 110$ GeV in the left panel and $M_{H^\pm} = 140$ GeV in the right panel.

We now investigate the characteristics of the finally allowed parameter sets. In Fig. 1, we show M_A vs M_H with the color code indicating the value of m_{12}^2 for $M_{H^\pm} = 110$ GeV (left panel) and $M_{H^\pm} = 140$ GeV (right panel). We first observe that m_{12}^2 is positive and not large: for example, $20 \text{ GeV} \lesssim \sqrt{m_{12}^2} \lesssim 120 \text{ GeV}$ when $M_{H^\pm} = 110$ GeV. The second important aspect is that the other new scalar bosons, H and A , cannot be too heavy. There exist upper bounds on their masses like $M_H, M_A \lesssim 570$ GeV. Once the charged Higgs boson is light, partial decoupling of new Higgs bosons is not feasible in type-I. Another intriguing feature is the correlation between M_H and M_A . If M_A is heavy ($\gtrsim 300$ GeV), M_H should be light. If M_H is heavy above 300 GeV, the pseudoscalar A should have an intermediate mass, $M_A \in [100, 150]$ GeV for $M_{H^\pm} = 110$ GeV and $M_A \in [140, 200]$ GeV for $M_{H^\pm} = 140$ GeV. A and H cannot be simultaneously heavy.

Of special importance is the parameter region of $M_A < m_h/2$ where the exotic Higgs decay $h \rightarrow AA$ is kinematically allowed. All the surviving parameters, consistent with the current Higgs precision data [69–74], yield $\mathcal{B}(h \rightarrow AA) \lesssim 10\%$. In detail, about 50% of the allowed parameter sets with $M_A < m_h/2$ predict $\mathcal{B}(h \rightarrow AA) \lesssim 1\%$ while about 20% yield $7\% \lesssim \mathcal{B}(h \rightarrow AA) \lesssim 10\%$. The ongoing LHC searches for the exotic Higgs decay are extremely important in

finding out the structure of type-I.

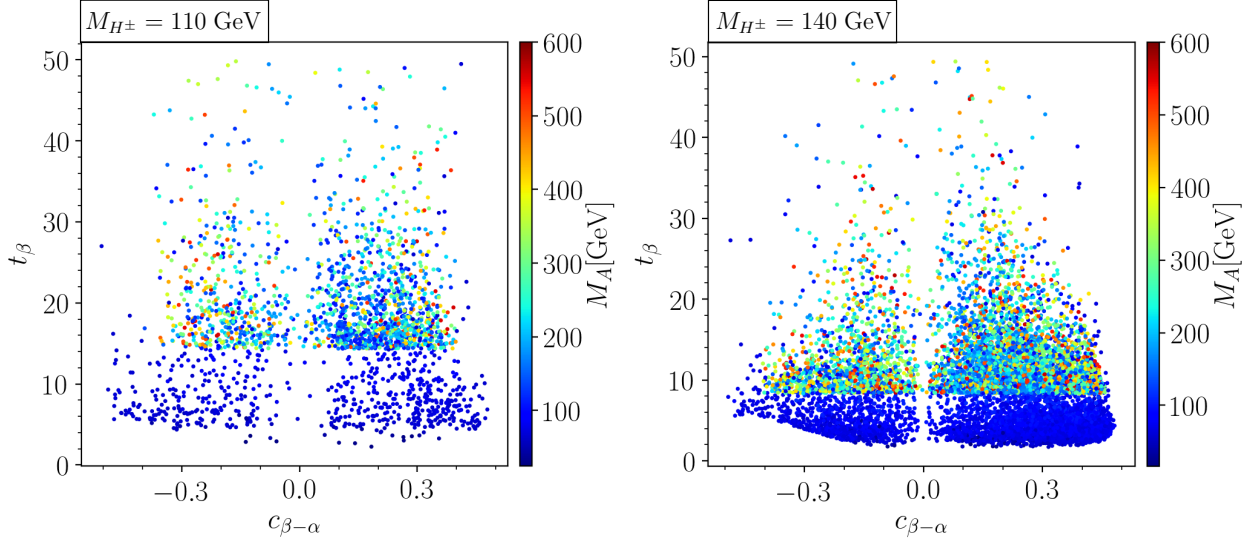


Figure 2: t_β vs $c_{\beta-\alpha}$ with the color code of M_A for $M_{H^\pm} = 110$ GeV (left panel) and $M_{H^\pm} = 140$ GeV (right panel).

Figure 2 shows t_β vs $c_{\beta-\alpha}$ for $M_{H^\pm} = 110$ GeV (left panel) and $M_{H^\pm} = 140$ GeV (right panel), with the color code indicating M_A . We observe that $t_\beta \lesssim 10$ is still allowed, as low as $t_\beta \sim 2$. It seems contradictory to the usual conclusion that no signal for the light H^\pm at the LHC demands large t_β in type-I. However, the conclusion is based on the assumption of $M_{H^\pm} \simeq M_H \simeq M_A$ so that the light H^\pm decays only into the SM fermions. Even though the mass degeneracy is motivated to satisfy the Peskin-Takeuchi oblique parameters, the current data in Eq. (11) leave some room for sizable mass differences, especially when the new Higgs bosons are not heavy. All of the surviving points with $t_\beta \lesssim 10$ incorporate light M_A , which opens the $H^\pm \rightarrow AW^{\pm(*)}$ mode. Consequently, $\mathcal{B}(H^\pm \rightarrow \tau\nu)$ reduces and the LHC constraint on $\mathcal{B}(t \rightarrow H^+b) \times \mathcal{B}(H^+ \rightarrow \tau\nu)$ can be evaded. If M_A is above the threshold of $H^\pm \rightarrow AW^{\pm(*)}$, t_β should be large, $t_\beta \gtrsim 15$ for $M_{H^\pm} = 110$ GeV and $t_\beta \gtrsim 9$ for $M_{H^\pm} = 140$ GeV. Finally, we observe that sizable deviation from the alignment limit is still possible in type-I. Indeed, the population of the allowed parameter points indicates the preference for $|c_{\beta-\alpha}| \in [0.1, 0.4]$. As a result, the model can accommodate $H \rightarrow WW/ZZ$, $A \rightarrow hZ$, and $H^\pm \rightarrow W^{\pm(*)}h$.

We move on to the next question of whether the new Higgs bosons prefer some specific decay modes. It is closely related to one of our goals, a complete roadmap for the light charged Higgs boson in type-I. The critical parameter is found to be M_A . In Fig. 3, we present the branching ratios of H^\pm vs M_A for $M_{H^\pm} = 110$ GeV (left panel) and $M_{H^\pm} = 140$ GeV (right panel), where the scattered points correspond to all the surviving parameter sets. We include the three-body decay of $AW^{\pm(*)}$.⁵ For $H^\pm \rightarrow q\bar{q}'$, we incorporate QCD radiative corrections at order α_s^2 in

⁵ The three-body decay of $H^\pm \rightarrow A^*W^\pm$ is negligible since the Yukawa couplings of A to $f\bar{f}$ are much smaller than the gauge couplings of the W^\pm boson.

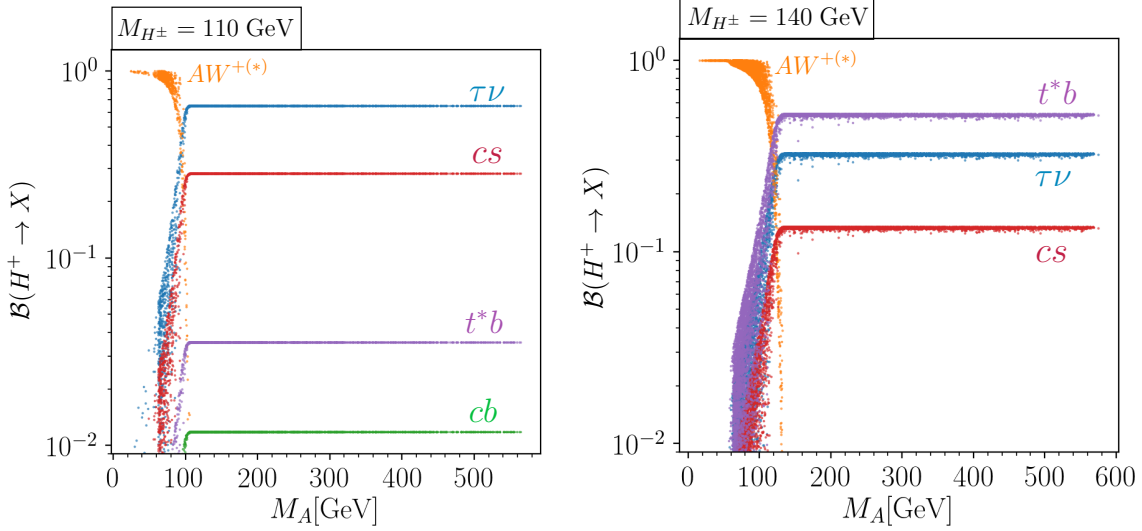


Figure 3: Branching ratios of the charged Higgs boson H^\pm vs M_A , predicted by all the surviving parameter points. We fix $M_{H^\pm} = 110$ GeV (left panel) and $M_{H^\pm} = 140$ GeV (right panel).

the $\overline{\text{MS}}$ scheme [75–77] by using 2HDMC [49]. For the running fermion masses in the Higgs couplings, we resum the leading logarithmic corrections to all orders with the renormalization scale of $\mu_R = M_{H^\pm}$ in the $\overline{\text{MS}}$ scheme.

Figure 3 clearly demonstrates strong correlation between $\mathcal{B}(H^\pm \rightarrow X)$ and M_A . For a light A below the AW^\pm threshold, $H^\pm \rightarrow AW^\pm$ is dominant. If the on-shell decay is possible, the branching ratio reaches almost 100%. The off-shell decay also has a sizable branching ratio. Large $\mathcal{B}(H^\pm \rightarrow AW^\pm)$ is attributed to the gauge coupling of the H^\pm - W^\mp - A vertex. As soon as M_A crosses over the kinematic threshold, $H^\pm \rightarrow \tau^\pm \nu$ mode becomes important, yielding $\mathcal{B}(H^\pm \rightarrow \tau \nu) \simeq 60$ (30)% for $M_{H^\pm} = 110$ (140) GeV. The hadronic modes such as $t^* b$ and cs are also substantial.

Figure 4 presents the branching ratios of A vs M_A for $M_{H^\pm} = 110$ GeV (left panel) and $M_{H^\pm} = 140$ GeV (right panel). We see a strong correlation between $\mathcal{B}(A \rightarrow X)$ and M_A . Below the threshold of $A \rightarrow H^\pm W^\mp$, $A \rightarrow b\bar{b}$ is the dominant decay mode, followed by $A \rightarrow gg$ and $A \rightarrow \tau^+ \tau^-$. Above the threshold, $H^\pm W^\mp$ is the main decay mode. Unexpected is sizable and almost constant $\mathcal{B}(A \rightarrow ZH)$ when $M_A \gtrsim 300$ GeV. The result is attributed to two factors: the A - Z - H vertex is favored by the alignment; a heavy M_A is permitted only for light M_H as shown in Fig. 1. $\mathcal{B}(A \rightarrow Zh)$ is suppressed by the factor $c_{\beta-\alpha}^2$. $\mathcal{B}(A \rightarrow t\bar{t})$ is also small because M_A above the kinematic threshold ($M_A > 2m_t$) requires large t_β which suppresses the top quark Yukawa coupling to A .

Unlike H^\pm and A , the heavy CP -even H shows the wide variety of decay patterns. In the left panel of Fig. 5, we present $\mathcal{B}(H \rightarrow X)$ vs M_H for $M_{H^\pm} = 110$ GeV. Eight decay modes ($\tau^+ \tau^-$, ZZ , $W^+ W^-$, $b\bar{b}$, gg , ZA , AA , and $H^\pm W^\mp$) are all mixed up, particularly when $M_H < M_{H^\pm} + m_W$. The complication is from the involvement of two model parameters, M_H and $c_{\beta-\alpha}$. Another important feature is that below the threshold of $H \rightarrow H^\pm W^\mp$, $H \rightarrow ZZ$ and

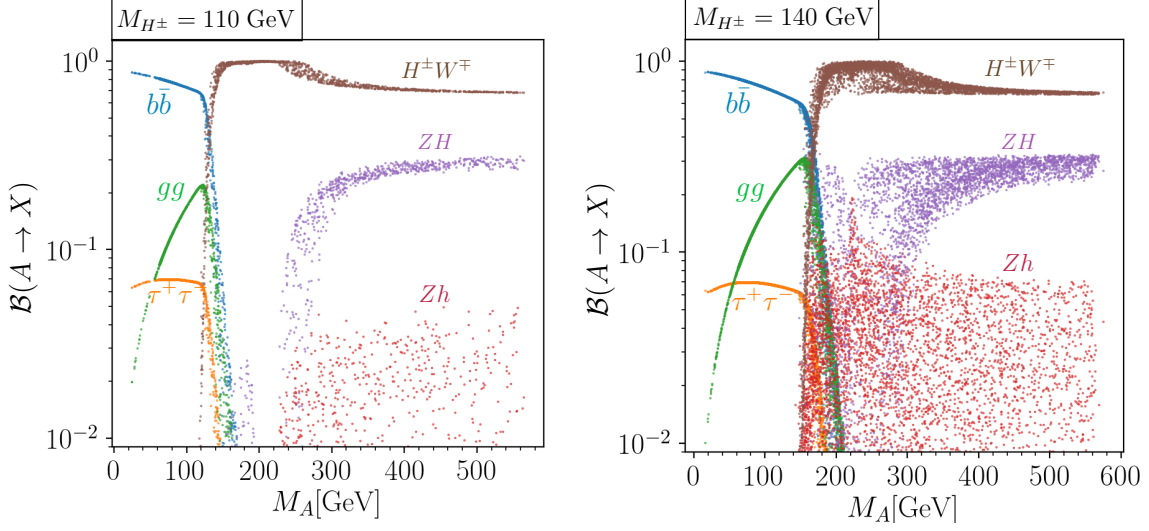


Figure 4: Branching ratios of the pseudoscalar boson A vs M_A for $M_{H^\pm} = 110$ GeV (left panel) and $M_{H^\pm} = 140$ GeV (right panel).

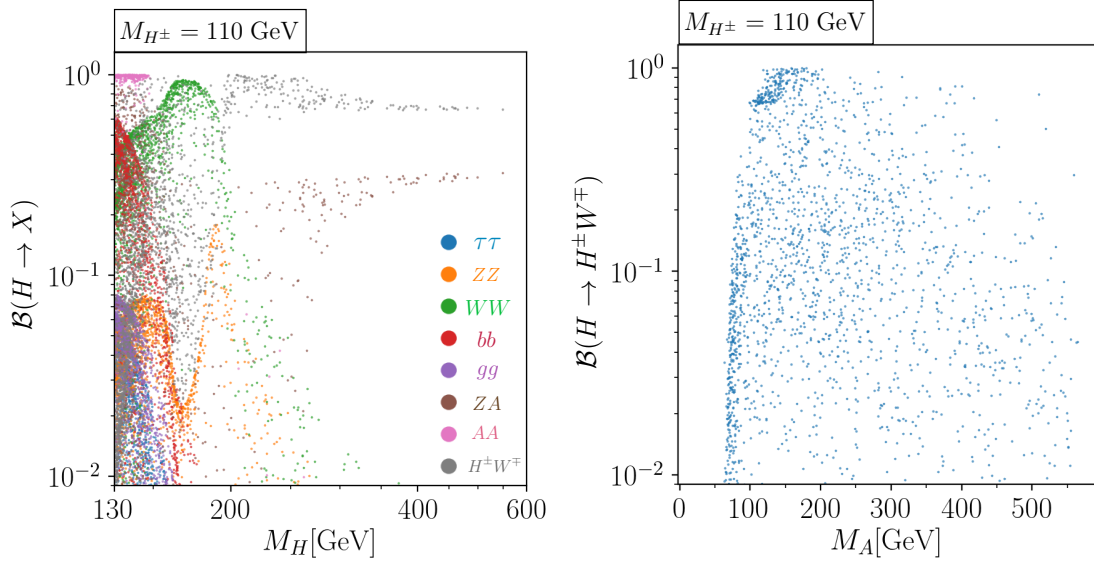


Figure 5: Branching ratios of H vs M_H (left panel), and $\mathcal{B}(H \rightarrow H^\pm W^\mp)$ vs M_A (right panel). We fix $M_{H^\pm} = 110$ GeV.

$H \rightarrow W^+W^-$ become substantial, which represents a deviation from the Higgs alignment limit. Above the threshold, $H \rightarrow H^\pm W^\mp$ is dominant in a large portion of the allowed parameter space (see the right panel of Fig. 5). The sizable H - H^\pm - W^\mp vertex provides a new production channel for the light charged Higgs boson in type-I.

	light A case	heavy A case
Target decay modes	$H^\pm \rightarrow AW^{\pm(*)}$	$H^\pm \rightarrow \tau\nu$
	$A \rightarrow b\bar{b}$	$A \rightarrow H^\pm W^\mp(*)$
	$H \rightarrow H^\pm W^\mp$	
Initial production	Final states	
$gg \rightarrow h/H/A \rightarrow H^\pm W^\mp$	$[b\bar{b}W^\pm]W^\mp$	$[\tau\nu]W^\pm$
$q\bar{q}' \rightarrow W^* \rightarrow H^\pm h$	$[b\bar{b}W^\pm]h$	$[\tau\nu]h$
$gg \rightarrow H \rightarrow AZ$	$b\bar{b}Z$	$[\tau\nu]W^\pm Z$
$gg \rightarrow HZ, q\bar{q} \rightarrow Z^* \rightarrow HZ$	$[b\bar{b}W^\pm]W^\mp Z$	$[\tau\nu]W^\pm Z$
$q\bar{q}' \rightarrow W^* \rightarrow H^\pm A$	$[b\bar{b}W^\pm]b\bar{b}$	$[\tau\nu][\tau\nu]W^\pm$
$q\bar{q}' \rightarrow W^* \rightarrow H^\pm H$	$[b\bar{b}W][b\bar{b}W]W^\pm \checkmark$	$[\tau\nu][\tau\nu]W^\pm$
$pp \rightarrow H^+ H^-$	$[b\bar{b}W^\pm][b\bar{b}W^\mp] \checkmark$	$[\tau\nu][\tau\nu] \checkmark$
$q\bar{q} \rightarrow Z^* \rightarrow HA$	$[b\bar{b}W^\pm]b\bar{b}W^\mp$	$[\tau\nu][\tau\nu]W^\pm W^\pm \checkmark$
$gg \rightarrow HH$	$[b\bar{b}W][b\bar{b}W]WW$	$[\tau\nu][\tau\nu]W^\pm W^\pm \checkmark$
$gg \rightarrow AA$	$b\bar{b}b\bar{b}$	$[\tau\nu][\tau\nu]W^\pm W^\pm \checkmark$

Table II: For the light and heavy A cases, the production channels of one or two charged Higgs bosons at the LHC, and the subsequent final states from the targeted decay modes of H^\pm , A , and H . The particles inside a square bracket in the final states are from the decay of one charged Higgs boson. The processes with a checkmark are expected to have high LHC discovery potential.

IV. PRODUCTION OF LIGHT CHARGED HIGGS BOSONS AT THE LHC

Based on the characteristics of the viable parameter space, we develop the search strategies for the light H^\pm in type-I. Since M_A is shown to be the key parameter, we divide the parameter space into two regions, the light A case and the heavy A case with the threshold of $M_A^{\text{threshold}} \simeq 100$ (120) GeV for $M_{H^\pm} = 110$ (140) GeV. When A is light, H^\pm dominantly decays into AW^\pm , and A decays into $b\bar{b}$. In the heavy A case, $H^\pm \rightarrow \tau\nu$ and $A \rightarrow H^\pm W^\mp$ are main decay modes. For the decays of H , we focus on $H \rightarrow H^\pm W^\mp$ to find new production channels of the light charged Higgs boson at the LHC.

In Table II, we summarize the possible production channels of the light H^\pm at the LHC, and the final states from the targeted decay modes of H^\pm , A , and H . To emphasize the decay products of a charged Higgs boson, we adopt the notation of a square bracket: $[ijk]$ denotes $H^\pm \rightarrow ijk$. To find the processes with high LHC discovery potential, we focus on the production of *two* charged Higgs bosons, which is more challenging for the background to mimic. We also consider the process with additional tagging particles that help to tame the background and increase the significance. And we avoid the signal processes with too small cross section, below about 1 fb. In Table II we put the checkmarks on the candidate processes.

In this regard, we study the following four channels:

- For the light A case,

– $[bbW][bbW]$:

The signal cross section is

$$\sigma_{[bbW][bbW]} = [\sigma(q\bar{q} \rightarrow H^+H^-) + \sigma(gg \rightarrow H^+H^-)] \times \mathcal{B}(H^+ \rightarrow AW^+)^2 \times \mathcal{B}(A \rightarrow b\bar{b})^2. \quad (13)$$

– $[bbW][bbW]W$:

The total signal rate is

$$\sigma_{[bbW][bbW]W} = [\sigma(q\bar{q}' \rightarrow W^{+*} \rightarrow H^+H) + \sigma(q\bar{q}' \rightarrow W^{-*} \rightarrow H^-H)] \times 2\mathcal{B}(H \rightarrow H^+W^-)\mathcal{B}(H^+ \rightarrow AW^+)^2\mathcal{B}(A \rightarrow b\bar{b})^2. \quad (14)$$

Four different charge conjugation combinations are to be summed.

- For the heavy A case,

– $[\tau\nu][\tau\nu](j)$:

The signal cross section is

$$\sigma_{[\tau\nu][\tau\nu]j} = [\sigma(pp \rightarrow H^+H^-) + \sigma(pp \rightarrow H^+H^-j)] \times \mathcal{B}(H^\pm \rightarrow \tau\nu)^2. \quad (15)$$

A pair of charged Higgs bosons is produced at the LHC via the Drell-Yan process and the gluon fusion.

– $[\tau\nu][\tau\nu]WW$:

We have

$$\begin{aligned} \sigma_{[\tau\nu][\tau\nu]WW} = & [\sigma(q\bar{q} \rightarrow Z^* \rightarrow HA) \times 4\mathcal{B}(H \rightarrow H^+W^-)\mathcal{B}(A \rightarrow H^+W^-) \\ & + \sigma(gg \rightarrow HH) \times 4\mathcal{B}(H \rightarrow H^+W^-)^2 \\ & + \sigma(gg \rightarrow AA) \times 4\mathcal{B}(A \rightarrow H^+W^-)^2] \times \mathcal{B}(H^+ \rightarrow \tau\nu)^2, \end{aligned} \quad (16)$$

where the factor of four covers four different combinations of charge conjugation. Half of them correspond to the same-sign W 's, $\tau^+\tau^+W^-W^-\nu\nu$ and $\tau^-\tau^-W^+W^+\nu\nu$.

Over the whole parameter space that satisfies all the theoretical and experimental constraints at Step-(i), Step-(ii), and Step-(iii), we calculate the parton-level cross sections at the LHC with $\sqrt{s} = 14$ TeV. We use MADGRAPH_AMC@NLO [78] with NNPDF31_LO parton distribution function (PDF) set [79]. The renormalization and factorization scales are set to $\mu_R = \mu_F = \sum_i (1/2)\sqrt{p_{T,i}^2 + m_i^2}$. Since the 2HDM UFO file in the MADGRAPH misses some important decay modes of new scalar bosons such as $H^\pm \rightarrow cs$ and $A \rightarrow gg$, we modified the values of the extra scalar decay widths in the MADGRAPH input cards to match the output of the 2HDMC [49]. In Fig. 6, we present the parton-level cross sections for $M_{H^\pm} = 110$ GeV (left panel) and $M_{H^\pm} = 140$ GeV (right panel). Here $[\tau\nu][\tau\nu]j_{30}$ denotes the pair production of

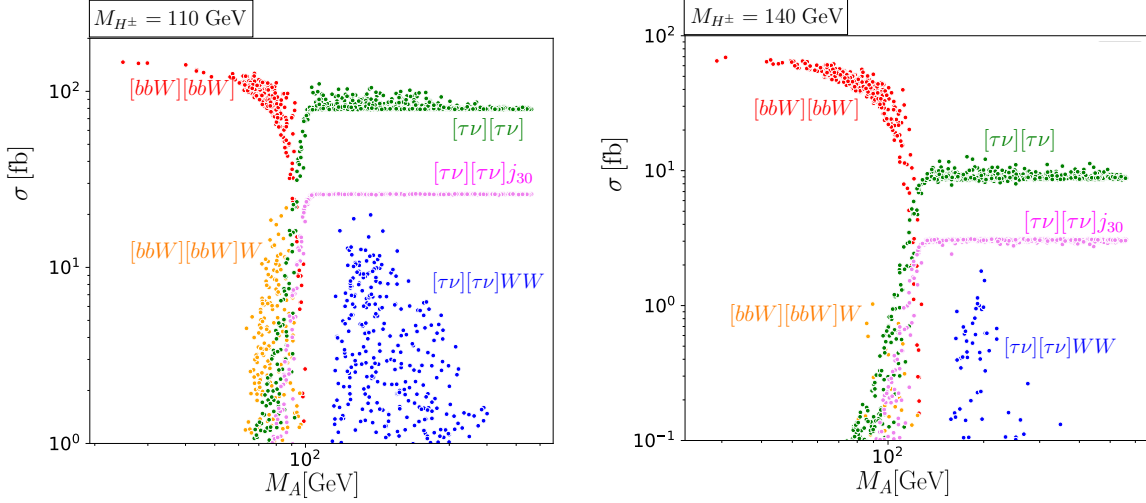


Figure 6: Parton-level cross sections of the signal in the final states of $[b\bar{b}W^+][b\bar{b}W^-]$, $[b\bar{b}W][b\bar{b}W]W$, $[\tau\nu][\tau\nu]$, $[\tau\nu][\tau\nu]j_{30}$, and $[\tau\nu][\tau\nu]WW$ at the 14 TeV LHC. The particles inside a square bracket represent the decay products of a charged Higgs boson, and j_{30} denotes a jet with $p_T^j > 30$ GeV. We consider $M_{H^\pm} = 110$ GeV (left panel) and $M_{H^\pm} = 140$ GeV (right panel).

charged Higgs bosons with one extra jet from initial state radiation (ISR). The subscript in j_{30} points out the additional requirement of $p_T^j > 30$ GeV. As shown below, including an extra-jet emission considerably improves the signal significance.

Figure 6 clearly demonstrates the crucial role of M_A in the LHC phenomenology of the light H^\pm in type-I. For $M_A < M_A^{\text{threshold}}$, only the process $pp \rightarrow H^+H^- \rightarrow [b\bar{b}W][b\bar{b}W]$ (red points) has sizable cross sections, which reaches about 100 fb for $M_{H^\pm} = 110$ GeV and about 80 fb for $M_{H^\pm} = 140$ GeV. An advantage of this process is that the cross sections have small variations over all the surviving parameters. There are two reasons. First, the main production of a charged Higgs boson pair, the Drell-Yan process, is determined solely by M_{H^\pm} . Second, the decays of $H^\pm \rightarrow AW^\pm$ and $A \rightarrow b\bar{b}$ are dominant for light M_A , irrespective to t_β (see Figs. 3 and 4).

When the light M_A approaches $M_A^{\text{threshold}}$, the signal rate of $[b\bar{b}W][b\bar{b}W]W^\pm$ (yellow points) can be substantial when various conditions fit exquisitely. The parameters with $M_A \simeq M_A^{\text{threshold}}$ strongly prefer heavy M_H : see Fig. 1. Then a large portion of the parameter space yields sizable branching ratio for $H \rightarrow H^\pm W^\mp$. The production of $q\bar{q}' \rightarrow W^* \rightarrow H^\pm H$, favored by the Higgs alignment, is followed by $H \rightarrow H^\pm W^\mp$ and $H^\pm \rightarrow AW^\pm$. The final state becomes $[b\bar{b}W][b\bar{b}W]W^\pm$.

As soon as M_A exceeds $M_A^{\text{threshold}}$, the cross section of $[b\bar{b}W][b\bar{b}W]$ rapidly drops and $pp \rightarrow H^+H^- \rightarrow [\tau\nu][\tau\nu]$ becomes dominant. The cross section of $[\tau\nu][\tau\nu]$ is almost constant because $\mathcal{B}(H^\pm \rightarrow \tau\nu)$ is nearly constant for heavy M_A . We also show the signal rate of $[\tau\nu][\tau\nu]j_{30}$ (magenta points). Although it is a $2 \rightarrow 3$ QCD process, $gq \rightarrow H^+H^-q$ is benefited by the high gluon luminosity. The extra-jet emission is known to be useful in improving the significance, particularly for rare NP processes [80]. Furthermore, it provides more kinematic control to

Signal	Benchmark point		Backgrounds
$[\tau\nu][\tau\nu]$	BP-1	$M_{H^\pm} = 110 \text{ GeV}, M_H = 138.6 \text{ GeV}, M_A = 120.7 \text{ GeV}$ $t_\beta = 16.8, s_{\beta-\alpha} = 0.975, m_{12}^2 = 1089.7 \text{ GeV}^2$	$Wjj, Zjj, t\bar{t}jj$ $WWjj, WZjj, ZZjj$
$[\tau\nu][\tau\nu]W_{\ell^\pm\nu}W_{\ell^\pm\nu}$	BP-2	$M_{H^\pm} = 110 \text{ GeV}, M_H = 138 \text{ GeV}, M_A = 145 \text{ GeV}$ $t_\beta = 18, s_{\beta-\alpha} = 0.999, m_{12}^2 = 1043 \text{ GeV}^2$	$W^+W^-W^-, W^-W^+W^+$ $t\bar{t}W^\pm, t\bar{t}Z, h_{\text{SM}}Z, ZZ$
$[bbW_{\ell\nu}][bbW_{qq'}]$	BP-3	$M_{H^\pm} = 110 \text{ GeV}, M_H = 134 \text{ GeV}, M_A = 29 \text{ GeV}$ $t_\beta = 3.9, s_{\beta-\alpha} = 0.967, m_{12}^2 = 533 \text{ GeV}^2$	$WW, ZZ, ZZb\bar{b}$ $t\bar{t}, tV, h_{\text{SM}}V, t\bar{t}h_{\text{SM}}/V$

Table III: Benchmark points for three target processes of a light charged Higgs boson at the HL-LHC. The main backgrounds are also listed, with $V = W^\pm, Z$.

suppress the backgrounds.

Finally, we exhibit the cross sections of $[\tau\nu][\tau\nu]WW$ (blue points), which become sizable for moderately heavy M_A , above $M_A^{\text{threshold}}$ but below about 250 GeV. The pseudoscalar mass in this range demands M_H above the threshold of $H \rightarrow H^\pm W^\mp$, as shown in Fig. 1. As a result, both A and H decay into $H^\pm W^\mp$ with a non-negligible branching ratio. The associated production of H and A mediated by Z , which is preferred by the Higgs alignment limit, leads to $[\tau\nu][\tau\nu]WW$. Note that the gluon-fusion productions of HA, HH , and AA also generate the same final state.

V. SIGNAL-BACKGROUND ANALYSIS FOR $[bbW][bbW]$, $[\tau\nu][\tau\nu]$, AND $[\tau\nu][\tau\nu]WW$

In the previous section, we calculated the parton-level cross sections of the proposed channels to probe the light H^\pm in type-I. Although their magnitudes are not small, the discovery potential depends on how efficiently we isolate the signal from the overwhelming backgrounds. In this section, we develop the search strategies for a fully-fledged signal-to-background optimization which relies upon sophisticated tools that include hard-scattering matrix elements, resonance decays, parton showers, hadronization, hadron decays, and a simplified detector's response. Targeting the HL-LHC, we perform detailed studies of the following three processes: $[\tau\nu][\tau\nu](j)$, $[\tau^\pm\nu][\tau^\pm\nu]W^\mp W^\mp$, and $[bbW][bbW]$. For each channel, we adopt the benchmark set in Table III. We also list the backgrounds. The benchmark points for $[\tau\nu][\tau\nu]$ and $[\tau\nu][\tau\nu]WW$ are representative of the process because all the allowed parameters yield similar signal rates. But the benchmark point for $[bbW][bbW]$ is chosen to maximize the signal rate.

Before getting into the detailed analysis for each process, we present the common ingredients. For the Monte Carlo event generation of the signal and backgrounds, we use the 2HDM UFO file [81] and MADGRAPH_AMC@NLO version 2.6.7. [78] with the NNPDF31_LO set of parton distribution functions [79]. As in the previous section, the input cards in the MADGRAPH_AMC@NLO are modified in accordance with the values of 2HDMC [49]. We use the default settings in the run-card of MADGRAPH5 such as $p_T > 10 \text{ GeV}$, $|\eta| < 2.5$, and $\Delta R(\ell, \ell) \geq 0.4$, where $\Delta R = \sqrt{(\Delta\eta)^2 + (\Delta\phi)^2}$. The resulting parton-level events are passed

to PYTHIA version 8.243 to add parton showering, hadronization, and hadron decays [82]. We perform a fast detector simulation of the signal and backgrounds using the DELPHES version 3.4.2 [83]. Jet is clustered according to the anti- k_T algorithm [84] with a jet radius $R = 0.4$. Since we demand to trigger at least one charged lepton, we do not include the pileup effects. We also turn off the multiple parton interactions from the soft QCD contribution at the level of PYTHIA 8. Under the above setup, we generate the signal and background events, which are to be called “Initial events” in what follows.

We now turn into the discussion of the object identification, which consists of τ -tagging, b -tagging, and a charged lepton. The quality of τ -tagging is crucial and vital for $[\tau\nu][\tau\nu]$ and $[\tau\nu][\tau\nu]WW$. A tau lepton that decays hadronically, denoted by τ_h in what follows, can be distinguished from a QCD jet by fewer particle multiplicity and more localized energy deposits. Recently, the τ_h -tagging efficiency has increased significantly with the improvements in π^0 reconstruction and multivariate discriminants [85]. At the DELPHES level, we set the τ_h -tagging efficiencies and the mistagging rates of a light jet (j) or the b jet as τ_h :⁶

$$\begin{aligned} P_{\tau \rightarrow \tau} &= 0.85, & P_{j \rightarrow \tau} &= 0.02, & \text{in the one-prong } \tau \text{ decays;} \\ P_{\tau \rightarrow \tau} &= 0.65, & P_{j, b \rightarrow \tau} &= 0.01, & \text{in the three-prong } \tau \text{ decays.} \end{aligned} \quad (17)$$

We also note that the sign of the electric charge of τ_h^\pm can be determined by the charged tracks.

The b -tagging is critical for all three processes. We employ b -tagging to remove the $t\bar{t}$ related backgrounds in the $[\tau\nu][\tau\nu]$ and $[\tau\nu][\tau\nu]WW$ and to improve the signal preselection for the $[bbW][bbW]$ process. In general, b -tagging is based on the so-called ghost-association technique [87] where a reconstructed jet is b -tagged if any B hadron with $p_T > 5$ GeV is found within $\Delta R = 0.3$ of the jet. In this connection, we first require that a candidate for a b jet should have minimal acceptance and trigger cuts of $p_T > 30$ GeV and $|\eta| < 2.5$. Then we apply the b -tagging efficiency and the mistag rates of the charm or light quark jet as a b -jet [88, 89]:

$$P_{b \rightarrow b} = 70\%, \quad P_{c \rightarrow b} = 10\%, \quad P_{j \rightarrow b} = 0.2\%. \quad (18)$$

For the lepton ($\ell^\pm = e^\pm, \mu^\pm$) identification, we demand the same rapidity of $|\eta_\ell| < 2.5$, but different p_T cuts for the electron and muon as $p_T^e > 17$ GeV and $p_T^\mu > 15$ GeV. To reduce the leptons from decays of heavy hadrons, we apply tight isolation criteria. For each charged lepton, we compute the isolation variable given by

$$I_\ell \equiv \frac{1}{p_T^\ell} \sum_i p_{T_i}, \quad (19)$$

where the sum runs over photon, (neutral and charged) hadrons within $\Delta R = 0.2$ (0.3) around the electron (muon) direction. In this analysis, we require $I_\ell < 0.06$.

⁶ The CMS collaboration has measured the misidentification probability of a b jet as τ_h by using the final states of $e\mu+$ jets in the $t\bar{t}$ events where the misidentified τ_h is dominated by the b jet [85]. In this paper, however, we take a conservative stance that the b jet has the same misidentification probability as the other QCD jets [86].

Finally, we calculate the signal significance including the background uncertainty, defined by [90]

$$\mathcal{S} = \left[2(N_s + N_b) \log \left(\frac{(N_s + N_b)(N_b + \delta_b^2)}{N_b^2 + (N_s + N_b)\delta_b^2} \right) - \frac{2N_b^2}{\delta_b^2} \log \left(1 + \frac{\delta_b^2 N_s}{N_b(N_b + \delta_b^2)} \right) \right]^{1/2}, \quad (20)$$

where N_s is the number of signal events, N_b is the number of total background events, and $\delta_b = \Delta_{\text{bg}} N_b$ is the uncertainty on the background yields.

A. $[\tau\nu][\tau\nu]$

The $[\tau\nu][\tau\nu]$ mode targets at the production of a charged Higgs boson pair, $pp \rightarrow H^+ H^-$, followed by $H^\pm \rightarrow \tau_h^\pm \nu$:

$$pp \rightarrow H^+ H^- \rightarrow \tau_h^+ \nu \tau_h^- \nu. \quad (21)$$

The final state consists of two hadronic τ 's and missing transverse energy. As shown in Fig. 6, this process covers most of the parameter space with $M_A > M_{H^\pm} - 10$ GeV.

At the 14 TeV LHC with the total integrated luminosity of $\mathcal{L}_{\text{tot}} = 3 \text{ ab}^{-1}$, we prepared the signal samples up to one merged jet using the MLM scheme based on k_T jet clustering algorithm [91]. The benchmark point BP-1 in Table III yields

$$\sigma(pp \rightarrow H^+ H^-) + \sigma(pp \rightarrow H^+ H^- j) = 0.35 \text{ pb}, \quad \mathcal{B}(H^\pm \rightarrow \tau^\pm \nu) = 0.652, \quad (22)$$

where we have imposed $p_T^j > 10$ GeV.

Now we cautiously assess the backgrounds. The backgrounds that we incorporated are based on the samples up to two jets merged with a parton shower, using the MLM scheme based on k_T jet clustering algorithm [91].

- $pp \rightarrow W + \text{jets}$ where one τ_h comes from W decay and the other τ_h from a jet misidentified as τ_h ;
- $pp \rightarrow Z/\gamma + \text{jets}$ consisting of $Z/\gamma(\rightarrow \tau\tau) + \text{jets}$ and $Z(\rightarrow \nu\nu) + \text{jets}$;
- $t\bar{t} + \text{jets}$;
- $VV' + \text{jets}$ including $WW + \text{jets}$, $WZ + \text{jets}$, and $ZZ + \text{jets}$.
- $tW + \text{jets}$ and $tZ + \text{jets}$.

Table IV describes the cut-flow of the number of events after the subsequent selection cuts. The ‘‘Basic cuts’’ consist of three.

- We veto any event with an electron, a muon, or a b -tagged jet. Most of the $t\bar{t} + \text{jets}$ backgrounds are rejected by the b -veto.

[$\tau\nu$][$\tau\nu$]						
Cut	W+jets	Z/ γ +jets	$t\bar{t}$ +jets	VV'+jets	N_b	N_s
Initial	6.2×10^{11}	4.39×10^{10}	1.33×10^9	4.41×10^8	6.65×10^{11}	1.04×10^6
Basic cuts	1.45×10^7	1.96×10^8	92929	271570	2.11×10^8	36413
$E_T^{\text{miss}} > 100$ GeV	298782	208799	11158	14478	533217	6448
$ \Delta\phi(\tau_1, \tau_2) > 2.4$	202117	36374	5914	5503	249908	3926
$\Delta R(\tau_1, \tau_2) < 3$	114240	8328	2926	2500	127994	2328
$M_{\tau_1\tau_2} > 300$ GeV	0	1054	182	183	1419	465
$p_T^{\tau_2} > 100$ GeV	0	737	121	121	979	347
$M_T^{\tau_2} > 50$ GeV	0	0	121	101	222	284

Table IV: Cut-flow chart of the number of events of the signal and backgrounds for the channel $pp \rightarrow H^+H^- \rightarrow [\tau_h^+\nu][\tau_h^-\bar{\nu}]$ at the 14 TeV LHC with the total integrated luminosity of $\mathcal{L}_{\text{tot}} = 3 \text{ ab}^{-1}$. Negligible backgrounds from tV +jets are omitted. More details about the selection cuts are in the text.

- We select the events including $\tau_h\tau_h$, $\tau_h\tau_h\tau_h$, or $\tau_h\tau_hj$. Here a τ_h jet is accepted when $p_T > 25$ GeV and $|\eta| < 2.5$.
- The electric charges of two τ_h jets should have opposite sign.

For the signal and background events after the basic cuts, we calculate various kinematic distributions. We show the distributions about missing transverse energy E_T^{miss} (top-left panel), $\Delta R(\tau_1, \tau_2)$ (top-right panel), the transverse momentum of the second-leading tau lepton $p_T^{\tau_2}$ (bottom-left panel), and the transverse mass of the second-leading tau lepton $M_T^{\tau_2}$ (bottom-right panel) in Fig. 7. τ_1 and τ_2 are ordered by the p_T such that $p_T^{\tau_1} > p_T^{\tau_2}$. M_T^τ is the transverse mass of a tau lepton, defined by

$$M_T^\tau = \sqrt{2|p_T^\tau||E_T^{\text{miss}}| \times \{1 - \cos(\phi_\tau - \phi_{\text{miss}})\}}, \quad (23)$$

where ϕ_τ and ϕ_{miss} are the azimuth angle of the τ lepton and the missing momentum, respectively. As shown in the top-left panel, E_T^{miss} plays a critical role in separating the signal from the background. The main backgrounds of Zjj and Wjj yield relatively soft E_T^{miss} , while the signal produces hard E_T^{miss} . For this reason, we enforce $E_T^{\text{miss}} > 100$ GeV. The other three distributions in Fig. 7 are the results after imposing $E_T^{\text{miss}} > 100$ GeV. Only about 0.2% of the backgrounds survive the E_T^{miss} selection, while about 18% of the signal events remain.

Based on the investigation of the kinematic distributions, we devise a search strategy summarized in the cutflow. One of the most efficient cuts is $M_{\tau_1\tau_2} > 300$ GeV, which removes about 99% of the backgrounds but 80% of the signal. In the signal, $M_{\tau_1\tau_2}$ tends to be high because two tau leptons originate from different ancestors (H^+ and H^-). The cut of $p_T^{\tau_2} > 100$ GeV

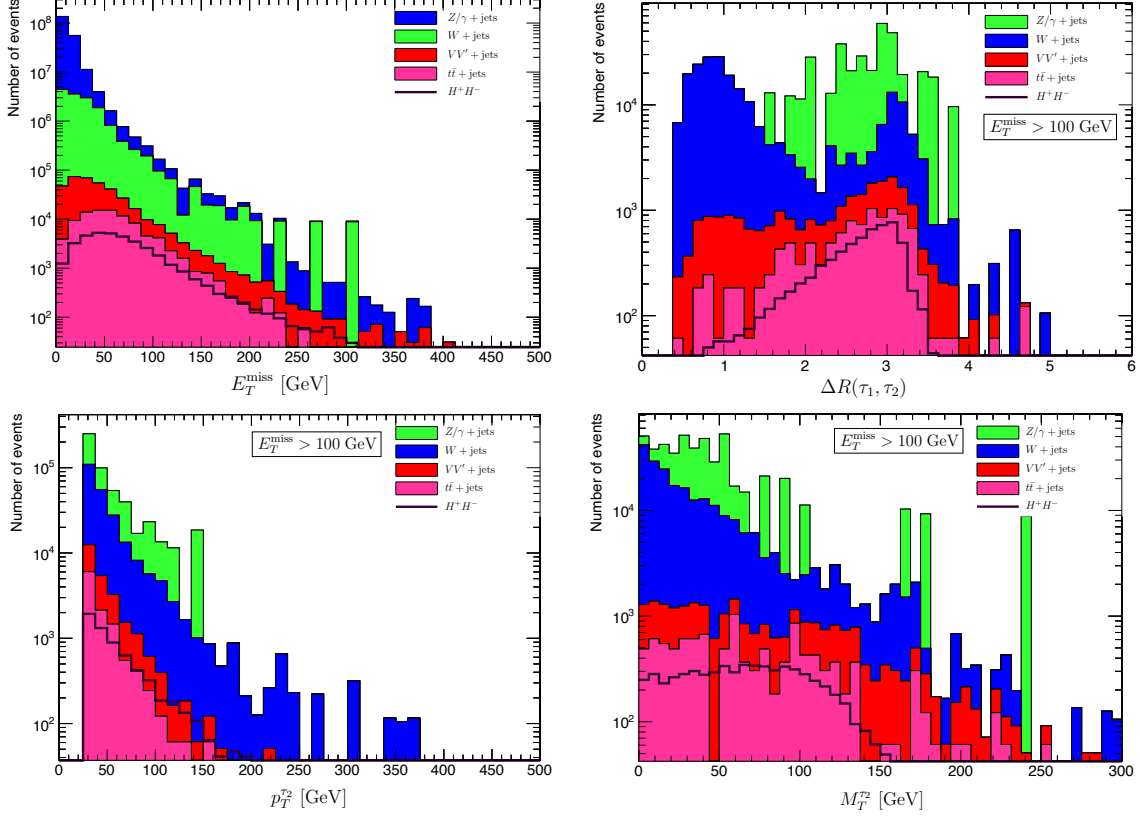


Figure 7: Kinematic distributions for the final state $[\tau\nu][\tau\nu]$ about missing transverse energy E_T^{miss} (top-left panel), $\Delta R(\tau_1, \tau_2)$ (top-right panel), the transverse momentum of the second-leading tau lepton $p_T^{\tau_2}$ (bottom-left panel), and the transverse mass of the second-leading tau lepton $M_T^{\tau_2}$ (bottom-right panel) at the 14 TeV LHC with the total integrated luminosity of $\mathcal{L}_{\text{tot}} = 3 \text{ ab}^{-1}$. The different background contributions are stacked on top of each other, and the expected signal is shown by black line. The distribution about E_T^{miss} is after imposing the basic cut, while the others are after imposing $E_T^{\text{miss}} > 100 \text{ GeV}$.

has certain advantage in separating the signal from the backgrounds, especially $t\bar{t}$ +jets and VV' +jets: surviving rate of the signal is about 75% while that of the total backgrounds is 68%. At this level, the dominant background is from Z/γ +jets. The final selection is on the transverse mass of the second-leading tau lepton, which aims at a τ associated with a neutrino. $M_T^{\tau_2} > 50 \text{ GeV}$ removes almost all the backgrounds from Z/γ +jets. At the final selection level, 284 signal events and 222 background events survive. The dominant backgrounds are $t\bar{t}$ +jets and VV' +jets. The significance without the background uncertainty is 19.7, which is very promising. Even with 10% background uncertainty, the significance is 8.2. Certainly, the HL-LHC can probe the light H^\pm through the $[\tau\nu][\tau\nu]$ final state if the mass M_A is above the decay threshold of $H^\pm \rightarrow A W^\pm$.

B. $[\tau^\pm\nu][\tau^\pm\nu]W^\mp W^\mp$

We consider the signal of

$$\begin{aligned} pp \rightarrow HA/HH/AA &\rightarrow H^-W^+H^-W^+ + \text{C.C.} \\ &\rightarrow \tau_h^-\nu\ell^+\nu\tau_h^-\nu\ell^+\nu + \text{C.C.}, \end{aligned} \quad (24)$$

where C.C. denotes the charge conjugate state. The final state consists of two same-sign leptons, two same-sign hadronic τ 's, and neutrinos. We consider the benchmark point BP-2 in Table III, where $\mathcal{B}(H \rightarrow H^\pm W^\mp) = 0.82$, $\mathcal{B}(A \rightarrow H^\pm W^\mp) = 0.88$, and $\mathcal{B}(H^\pm \rightarrow \tau^\pm \nu) = 0.65$. Drell-Yan production of HA is dominant over the gluon fusion production of HH and AA : $\sigma(q\bar{q} \rightarrow HA) = 75.5$ fb, $\sigma(gg \rightarrow HH) = 0.68$ fb, and $\sigma(gg \rightarrow AA) = 0.80$ fb. Therefore, we only generate the signal sample through $q\bar{q} \rightarrow HA$.

For the final state $\tau_h^-\tau_h^-\ell^+\ell^+E_T^{\text{miss}}$, the backgrounds are as follows:

- $pp \rightarrow t\bar{t} + W^+ \rightarrow b\ell^+\nu\bar{b}\tau^-\nu + \ell^+\nu$ where one of two b jets or a jet from QCD showering is misidentified as τ_h .
- $pp \rightarrow W^-W^+W^+ \rightarrow \tau_h^-\nu\ell^+\nu\ell^+\nu$ where a jet from showering is misidentified as τ_h .
- $pp \rightarrow ZZ \rightarrow \tau_{\ell^+}^+\tau_h^-\tau_{\ell^+}^+\tau_h^-$ where τ_ℓ denotes the leptonic decaying τ .
- $pp \rightarrow t\bar{t} + Z \rightarrow b\ell^+\nu\bar{b}\tau^-\nu + \tau_{\ell^+}^+\tau^-$.
- $pp \rightarrow h_{\text{SM}} + Z \rightarrow \tau_{\ell^+}^+\tau_h^- + \tau_{\ell^+}^+\tau_h^-$.

We also include the backgrounds for the charge conjugate signal state.

For event selection, we take the following steps. The ‘‘Basic cuts’’ consist of two.

- We require two same-sign charged leptons and two same-sign hadronic τ 's with $p_T^{\ell,\tau} > 20$ GeV and $|\eta_{\ell,\tau}| < 2.5$.
- The electric charge of two same-sign leptons should be opposite to that of two same-sign tau leptons.

After the basic cuts, the signal rate is considerably reduced. The resulting acceptance times efficiency, $\mathcal{A} \times \epsilon$, is about 3%. But the reduction of the total backgrounds is more severe with $\mathcal{A} \times \epsilon \simeq 0.3\%$. The basic cuts are most effective in the WWW background process since it is difficult for a QCD showering jet (mistagged as τ_h) to satisfy the requirement for the p_T and electric charge. The second selection is the b -jet veto. We reject the event including any b -tagged jet with $p_T^b > 30$ GeV and $|\eta_b| < 2.5$. It is designed to suppress the $t\bar{t}W$ and $t\bar{t}Z$ backgrounds, which results in a roughly 80% cut. On the contrary, the events from signal and other backgrounds remain almost intact. At this level, the significance without the background uncertainty is about 2.

$[\tau\nu][\tau\nu]\ell^\pm\nu\ell^\pm\nu$							
Cut	$t\bar{t}W$	$WWWW$	ZZ	$t\bar{t}Z$	$h_{\text{SM}}Z$	N_b	N_s
Initial	4560	1290	16567	1825	1407	25649	426
Basic cuts	15.14	0.63	35.37	17.04	6.42	74.6	15.6
b -jet veto	2.7	0.62	34.97	3.42	6.35	48.06	15.43
$E_T^{\text{miss}} > 45$ GeV	2.07	0.47	7.47	2.64	2.09	14.74	10.73
$p_T^{\ell(\text{lead})} < 70$ GeV	0.94	0.19	5.33	1.53	1.43	9.42	9.59
$p_T^{\tau(\text{lead})} > 40$ GeV	0.77	0.15	4.36	1.25	1.29	7.82	9.09
$0.4 < \Delta R(\ell, \tau)_1 < 0.8$	0.17	0.03	1.49	0.38	0.37	2.44	6.56
$M(\ell, \tau)_1 < 60$ GeV	0.16	0.03	1.31	0.35	0.35	2.2	6.43
$0.4 < \Delta R(\ell, \tau)_2 < 3.0$	0.1	0.01	1.24	0.28	0.35	1.98	6.36
$M(\ell, \tau)_2 < 70$ GeV	0.04	0	1.04	0.14	0.24	1.46	6.04

Table V: Cut-flow chart of the number of events for the final state $[\tau^\pm\nu][\tau^\pm\nu]\ell^\mp\nu\ell^\mp\nu$ at the 14 TeV LHC with the total integrated luminosity of $\mathcal{L}_{\text{tot}} = 3 \text{ ab}^{-1}$. Details about “Basic cuts” and the selection are in the text.

To devise more sophisticated selections, we show in Fig. 8 the kinematic distributions of the signal and backgrounds about missing transverse energy E_T^{miss} (top-left panel), the transverse momentum of the leading lepton $p_T^{\ell(\text{lead})}$ (top-right panel), the angular separation $\Delta R(\ell, \tau)_1$ (bottom-left panel), and the invariant mass $M(\ell, \tau)_2$ (bottom-right panel). The results are based on the events passing the basic cuts and b -jet veto. The first decisive cut is from the E_T^{miss} distribution. Both ZZ and $h_{\text{SM}}Z$ backgrounds have lower E_T^{miss} than the signal. We take $E_T^{\text{miss}} > 45$ GeV as the third selection, removing about 70% of ZZ and $h_{\text{SM}}Z$ backgrounds. The next important selection comes from the $p_T^{\ell(\text{lead})}$ distribution (top-right panel) where $\ell^{(\text{lead})}$ denotes the lepton with the largest p_T . $p_T^{\ell(\text{lead})}$ in the signal is softer than that in most of the backgrounds, while $p_T^{\tau(\text{lead})}$ in the signal is relative harder. In this regard, we select the events with $p_T^{\ell(\text{lead})} < 70$ GeV and $p_T^{\tau(\text{lead})} > 40$ GeV.

The final four selections in Table V are motivated by the characteristic of the signal $pp \rightarrow H + A \rightarrow H_{\tau^+\nu}^+ W_{\ell^-\nu}^- + H_{\tau^+\nu}^+ W_{\ell^-\nu}^-$. Two same-sign charged leptons in the signal come from different mother particles, H and A . To make the best use of the feature, we first select a pair of ℓ and τ with minimal $\Delta R(\ell_i, \tau_j)$, and call the pair $(\ell, \tau)_1$. The remaining pair of lepton and τ is $(\ell, \tau)_2$. In the bottom-left panel of Fig. 8, we show the distribution of the angular distance between the lepton and τ inside $(\ell, \tau)_1$. The bottom-right panel presents the distribution of the invariant mass of the lepton and τ inside $(\ell, \tau)_2$. The signal is mainly populated in the regions of low $\Delta R(\ell, \tau)_{1,2}$ and low $M(\ell, \tau)_{1,2}$, compared with the backgrounds. So we make the final four selections of $0.4 < \Delta R(\ell, \tau)_1 < 0.8$, $M(\ell, \tau)_1 < 60$ GeV, $0.4 < \Delta R(\ell, \tau)_2 < 3.0$, and $M(\ell, \tau)_2 < 70$ GeV. They are efficient to control the whole backgrounds, especially the $t\bar{t}W$,

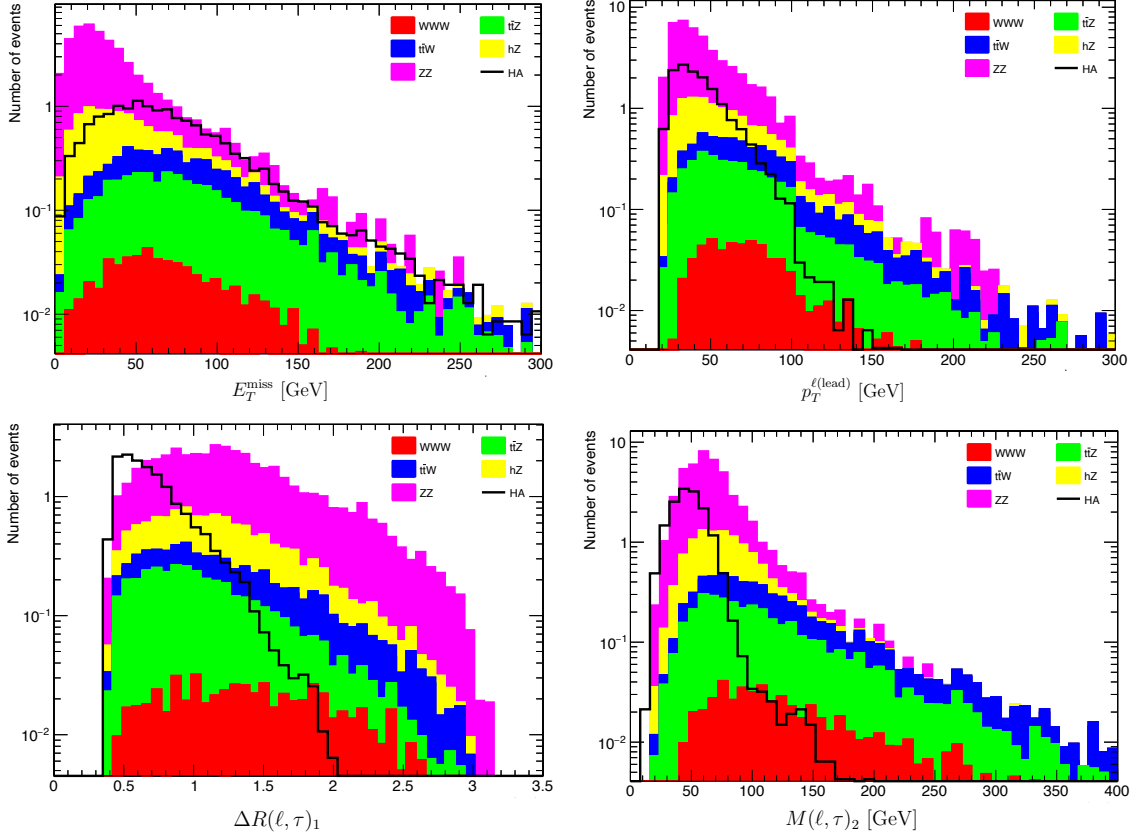


Figure 8: Kinematic distributions for the final state $[\tau\nu][\tau\nu]\ell^\pm\nu\ell^\pm\nu$ at the 14 TeV LHC with the total integrated luminosity of $\mathcal{L}_{\text{tot}} = 3 \text{ ab}^{-1}$. The results shown are after the basic cuts and b -jet veto. The different background contributions are stacked on top of each other, and the expected signal is shown by black line. Four representative distributions are presented on the missing transverse energy E_T^{miss} (top-left panel), the leading charged lepton transverse momentum $p_T^{\ell(\text{lead})}$ (top-right panel), the angular separation between the lepton and the τ in the $(\ell, \tau)_1$ pair (bottom-left panel), and the invariant mass of the lepton and the τ in the $(\ell, \tau)_2$ pair (bottom-right panel).

$t\bar{t}Z$, and WWW backgrounds. As $2 \rightarrow 3$ scattering processes, these backgrounds yield wide opening angles, which fail the final four selections. The ZZ and $h_{\text{SM}}Z$ backgrounds also prefer wide opening angles because of lighter masses of Z and h_{SM} than H and A . About 80% of these two backgrounds are removed.

After all of the above selections, 6.04 signal events and 1.46 background events (mostly ZZ background) are left. The significance without the background uncertainty is 3.53. If we include 10% background uncertainty, the significance slightly reduces to 3.48. Marginally, the HL-LHC can probe the light H^\pm through the signal of two same-sign charged leptons and two same-sign hadronic τ 's in the $[\tau\nu][\tau\nu]WW$ final state.

C. $[bbW][bbW]$

The $[bbW][bbW]$ process targets the production of a pair of charged Higgs bosons, followed by $H^\pm \rightarrow AW^{\pm(*)}$

$$pp(q\bar{q}/gg) \rightarrow H^+H^- \rightarrow AW^+AW^- \rightarrow b\bar{b}\ell^+\nu_\ell b\bar{b}q\bar{q}' + \text{C.C.} \quad (25)$$

We consider the benchmark point BP-3 in Table III where the cross sections for the signal process are

$$\text{BP-3: } \sigma(q\bar{q} \rightarrow H^+H^-) = 185.4 \text{ fb}, \quad \sigma(gg \rightarrow H^+H^-) = 25.6 \text{ fb}. \quad (26)$$

The cross section of loop-induced gluon fusion production is about 10% of the Drell-Yan production cross section. For the decay of WW , we consider the semi-leptonic decays. Then the backgrounds are as follows:

- $pp \rightarrow h_{\text{SM}}(\rightarrow b\bar{b})V + \text{jets}$ where the jets from the QCD showering are misidentified as b jets;
- $pp \rightarrow tV + t\bar{t}h_{\text{SM}} + t\bar{t}V$;
- $VV' + \text{jets}$;
- $ZZ + b\bar{b}$;
- $t\bar{t} + \text{jets}$.

At the LHC, $[bbW][bbW]$ is the most challenging process to probe the light H^\pm in type-I. The signal significance at the final selection shall be shown to be very small, far below the discovery level. Nevertheless, we present our investigation of all the available kinematic distributions and the effects of various kinematic cuts, hoping they help the future study. Some of the key distributions are shown in Fig. 9. First, we apply the “Basic cuts”, consisting of three selections.

- We select events if they contain exactly one charged lepton with $p_T^\ell > 25 \text{ GeV}$ and $|\eta| < 2.5$.
- We apply a veto on hadronically decaying tau leptons. Events should not contain any τ_h with $p_T > 20 \text{ GeV}$.
- $E_T^{\text{miss}} > 30 \text{ GeV}$.

After the basic cut, the signal significance without the background uncertainty is 4.81. As soon as we include the background uncertainty, however, the significance drops quickly, e.g., into 0.03 with $\Delta_{\text{bg}} = 1\%$. We need to reduce the background events.

We impose the cuts on the number of jets and b jets, $N_j \geq 4$ and $N_b \geq 2$, which is a key discriminator between the signal and background. In the signal, the number of jets is at least

$[b\bar{b}W][b\bar{b}W]$						
Cut	$h_{\text{SM}}V+\text{jets}$	$tV + t\bar{t}h_{\text{SM}}/V$	$VV + ZZbb$	$t\bar{t} + \text{jets}$	N_b	N_s
Initial	6.09×10^6	97.4×10^6	440.9×10^6	1.34×10^9	1.90×10^9	6.33×10^5
Basic cuts	4.27×10^5	15.1×10^6	46.42×10^6	206.42×10^6	2.69×10^8	8.01×10^4
$N_{\text{jets}} \geq 4, N_b \geq 2$	1.06×10^4	1.0×10^6	1.52×10^5	55.56×10^6	5.67×10^7	1.06×10^4
$M_T^W < 150 \text{ GeV}$	1.04×10^4	9.65×10^5	1.45×10^5	54.11×10^6	5.54×10^7	1.03×10^4
$M_{b_1 b_2} < 100 \text{ GeV}$	5.86×10^3	4.59×10^5	1.13×10^5	20.29×10^6	2.09×10^7	7.21×10^3
$p_T^{\ell(\text{lead})} < 350 \text{ GeV}$	5.85×10^3	4.59×10^5	1.13×10^5	20.28×10^6	2.08×10^7	7.21×10^3
$p_T^{\text{jet}} < p_T^{j,\text{max}}$	5.81×10^3	4.56×10^5	1.10×10^5	20.18×10^6	2.08×10^7	7.11×10^3
$E_T^{\text{miss}} < 0.7H_T$	5.72×10^3	4.49×10^5	1.09×10^5	20.00×10^6	2.06×10^7	7.06×10^3
top veto	5.11×10^3	4.14×10^5	1.00×10^5	18.67×10^6	1.92×10^7	6.78×10^3
cuts on M_{bbjj} and M_{bb}	2.20×10^2	1.45×10^4	2.49×10^3	6.08×10^5	6.25×10^5	3.90×10^2
$H_T < 400 \text{ GeV}$	1.92×10^2	1.21×10^4	1.84×10^3	5.18×10^5	5.33×10^5	3.08×10^2
$N_b = 3$	3.2×10^1	1.16×10^3	1.54×10^2	7.12×10^4	7.25×10^4	5.73×10^1
$N_b = 4$	0	1.40×10^2	0	6.08×10^3	6.23×10^3	1.42×10^1

Table VI: Cut-flow chart of the number of events of the signal and backgrounds for the channel $[b\bar{b}W][b\bar{b}W]$ at the 14 TeV LHC with the total integrated luminosity of $\mathcal{L}_{\text{tot}} = 3 \text{ ab}^{-1}$. Details about the selections are in the text.

six wherein four of them are b jets. But a large portion of the b jets from a light A are too soft to pass the jet selection threshold. Therefore, we impose a looser jet selection such that the events contain at least four jets and at least two b -jets. This selection, by itself, reduces the number of $t\bar{t}$ events by a factor of 4 and the signal by a factor of 8.

The charged lepton in the signal comes from the W decay. To take the full advantage of the feature, we pair the charged lepton with the missing transverse energy and construct the transverse mass M_T^W , defined by

$$M_T^W = \sqrt{2|p_T^\ell||E_T^{\text{miss}}| \times (1 - \cos \Delta\phi)}, \quad (27)$$

where $\Delta\phi = \phi_\ell - \phi_{\text{miss}}$. We require $M_T^W < 150 \text{ GeV}$. But it is not efficient since the charged lepton in the backgrounds involving top quarks comes from W also. Another characteristic of the signal is that two b jets come from a common ancestor. In the background, they are from different ancestors. We impose a condition on the invariant mass of the leading b jet (b_1) and the subleading b jet (b_2) such that $M_{b_1 b_2} < 100 \text{ GeV}$. This selection is effective to suppress the $t\bar{t} + \text{jets}$ (from $\sim 54\text{M}$ events to $\sim 20\text{M}$ events).

Further requirements are on the transverse momenta of the charged lepton and jets. First, we select events if the transverse momentum of the leading charged lepton is smaller than 350 GeV.

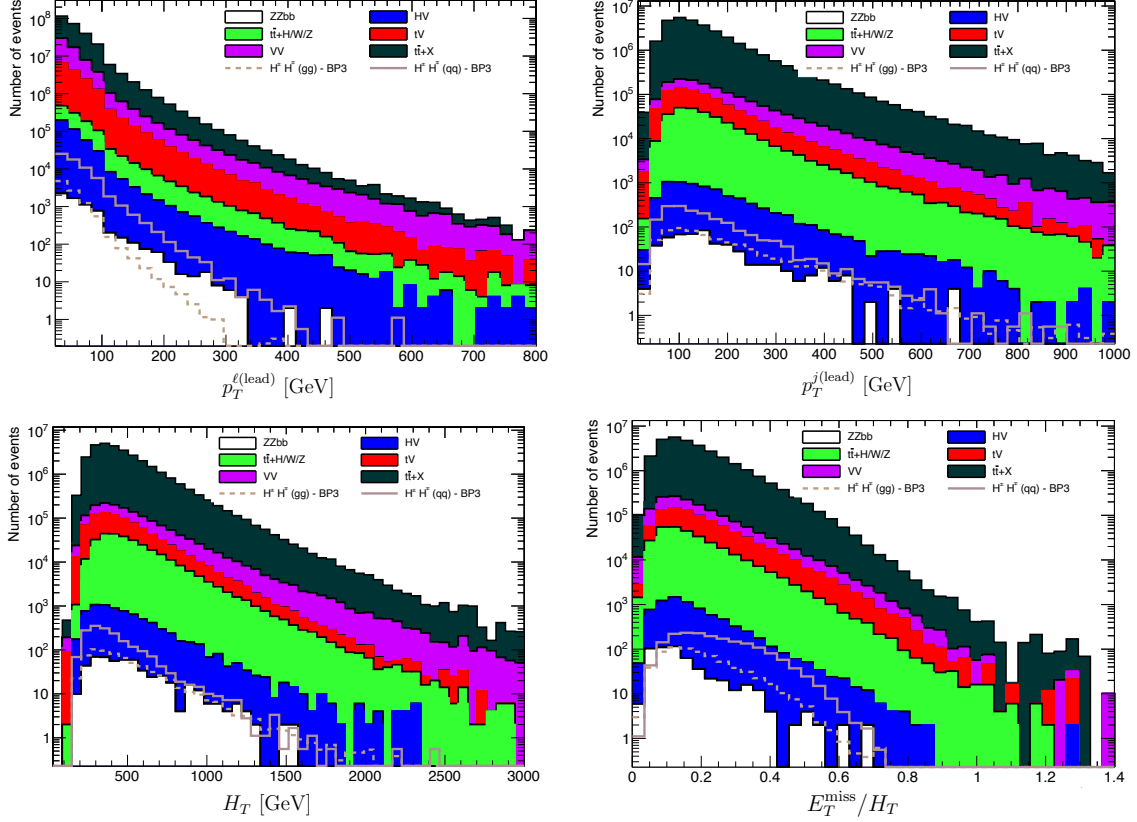


Figure 9: Examples for few selected distributions which we used in the signal-to-background optimization analysis: the leading jet transverse momentum (top-left panel); the leading lepton transverse momentum (top-right panel); H_T , the scalar sum of jet transverse momenta (bottom-left panel); the ratio of missing transverse energy to H_T (bottom-right panel). The backgrounds shown here correspond to $ZZbb$ (white), HV (blue), $t\bar{t} + H/W/Z$ (green), tV (red), VV (magenta) and $t\bar{t} + \text{jets}$ (dark green). In the same canvas, we show the $gg \rightarrow H^+H^-$ (dashed line) and $q\bar{q} \rightarrow H^+H^-$ (solid line) for BP-3 (light sienna).

Second, we require that the transverse momentum of a jet be smaller than $p_T^{j,\max}$, defined by $p_T^{j,\max} = 500, 350, 250, 150$ GeV for the leading, subleading, third, and fourth jet, respectively, regardless of whether they are b -tagged or not. Unfortunately, the cuts on $p_T^{\ell,j}$ hardly separate the signal from the backgrounds since basically the shapes of the $p_T^{\ell,j}$ distributions are very similar: see the top panels in Fig. 9.

Now we investigate the scalar sum of transverse momenta of jets, defined by

$$H_T = \sum_{i \in \text{jets}} p_T^i, \quad (28)$$

of which the distributions for the signal and backgrounds are in the bottom-left panel of Fig. 9. The background processes produce a hard H_T spectrum, while the signal has a softer spectrum. With the hope that some correlations of various energy observations (such as E_T^{miss} and the effective mass M_{eff}) to H_T may suppress the backgrounds, we examine the distributions of E_T^{miss}/H_T , $(E_T^{\text{miss}} + p_T^\ell)/H_T$, $E_T^{\text{miss}}/M_{\text{eff}}$, and $(E_T^{\text{miss}} + p_T^\ell)/M_{\text{eff}}$. Here $M_{\text{eff}} = p_T^\ell + E_T^{\text{miss}} + H_T$.

Since all of them give almost the same results, we choose $E_T^{\text{miss}}/H_T < 0.7$ as a representative: see the bottom-right panel of Fig. 9.

Since the backgrounds involving $t\bar{t}$ are still dominant, we further apply a top quark veto. Aiming at hadronically decaying top quark candidates, we construct W -candidates from any two jets with $p_T > 25$ GeV and $\Delta R(j_1, j_2) < 1.5$. Then, we veto events if any additional b jet with $p_T > 30$ GeV and $\Delta R(W_{jj}, b) < 1.5$ satisfies

$$X_{tt} \equiv \sqrt{\left(\frac{M_{jj} - M_W}{0.1M_{jj}}\right)^2 + \left(\frac{M_{jjb} - m_t}{0.1M_{jjb}}\right)^2} < 3.2, \quad (29)$$

for any possible combination. Next, we select hadronically decaying charged Higgs candidates. First, we construct two dijet systems, jj from the decay of the W -boson and bb from the decay of A . The dijet is formed if two jets are within $\Delta R < 1.5$. The two dijets, jj and $b\bar{b}$, are then combined to form a charged Higgs candidate, while the $b\bar{b}$ dijet system is to form A . Combining these, we require

$$|M_{jjbb} - M_{H^\pm}| < 10 \text{ GeV}, \quad |M_{bb} - M_A| < 10 \text{ GeV}. \quad (30)$$

Finally we demand that the H_T variable be smaller than 400 GeV.

The last discussion is on categorizing the events according to the number of b jets. At the end of the selection ($H_T < 400$ GeV), 236 signal events remained in the $N_b = 2$ region, 57 events in the $N_b = 3$ region and 14 events in the $N_b = 4$ region. The resulting significance is very small, about 0.2–0.4 after these selections. It turns out that more work is needed to refine the selection and to enhance the significance using deep-learning algorithms for example. Furthermore, we expect better perspective at electron-positron colliders at $\sqrt{s} = 250$ GeV where we expect almost background free environment, thanks to the absence of $t\bar{t}$ backgrounds.

VI. CONCLUSIONS

In the framework of the type-I 2HDM, we have comprehensively studied the phenomenology to set a full roadmap for the light charged Higgs boson. The existing constraint of $b \rightarrow s\gamma$ puts a very stringent lower bound on the mass of the charged Higgs boson in type-II and type-Y, as $M_{H^\pm} \gtrsim 580$ GeV. That is why we focus on type-I here. Imposing the light mass for the charged Higgs boson severely limits type-I, even without any assumptions on the model parameters, because of existing electroweak precision data, Higgs data, $b \rightarrow s\gamma$, and direct searches at the LEP, Tevatron, and LHC. The masses and couplings of the other Higgs bosons, A and H , are considerably restricted: (i) M_A and M_H are below about 580 GeV; (ii) there is a significant correlation between M_A and M_H (e.g., M_A and M_H cannot be simultaneously heavy); (iii) a light M_A allows small $\tan\beta$; (iv) the current data still permit substantial deviation from the Higgs alignment.

We rummaged among the finally allowed parameter space and found that the critical parameter is the mass of the pseudoscalar Higgs boson A . When AW^\pm is beyond the decay threshold

of the charged Higgs boson, H^\pm decays into a fermion pair, mainly into $\tau^\pm\nu$. Since only large $\tan\beta(\gtrsim 10)$ is allowed when M_A is heavy, the conventional production channel in the search for the light H^\pm , via the top quark decay, is not helpful. We found that the pair production of charged Higgs bosons has higher discovery potential. The associated production of H and A , followed by $H/A \rightarrow H^\pm W^\mp$, is also efficient to probe the light H^\pm . When AW^\pm is below the decay threshold of the charged Higgs boson, H^\pm will mostly decay into AW^\pm and A into $b\bar{b}$. Based on these characteristics, we assessed the detection significance of light charged Higgs bosons in three final states, $[\tau\nu][\tau\nu]$, $[\tau\nu][\tau\nu]\ell^\pm\nu\ell^\pm\nu$, and $[b\bar{b}W][b\bar{b}W]$. While we enjoy a large significance for the first final state and a reasonable significance for the second final state, the last one suffers from huge $t\bar{t}$ related backgrounds.

Before we close, a few comments are offered as follows:

1. The decay of the charged Higgs boson into AW^\pm depends on the gauge coupling, which is independent of Yukawa couplings, in contrast to fermionic decays. Once kinematically allowed, therefore, $H^\pm \rightarrow AW^\pm$ dominates over the fermionic modes. Thus, the mass of the pseudoscalar Higgs boson is a crucial factor in searching for the charged Higgs boson.
2. The golden channel for the light Higgs boson is $pp \rightarrow H^+H^- \rightarrow [\tau^+\nu][\tau^-\bar{\nu}]$ when the decay into AW^\pm is kinematically suppressed. Its signal rate enjoys a large significance. The benchmark point BP-1 that we illustrated gives a typical size of the cross sections in the allowed parameter space, thus the significance of other allowed parameter sets would not be substantially different. New techniques for improving the τ -tagging using multivariate discriminants and the measurement of the τ charge will further enhance the significance.
3. On the other hand, when the decay into AW^\pm is kinematically allowed, the decay chain $pp \rightarrow H^+H^- \rightarrow [AW^+][AW^-] \rightarrow [b\bar{b}\ell^+\nu][b\bar{b}q\bar{q}]$ is dominant in type-I but suffers the huge background from $t\bar{t}$ +jets. For this case, we do not get any significant sensitivity. We notice that this channel can be tested in the future electron-positron colliders at center-of-mass energy of 250 GeV due to the absence of the $t\bar{t}$ backgrounds.

Acknowledgments

K.C. would like to thank Professor Wai-Yee Keung of University of Illinois at Chicago for hospitality. K.C. was supported by MoST with grant numbers MoST-107-2112-M-007-029-MY3 and MOST-110-2112-M-007-017-MY3. The work of AJ is supported by a KIAS Individual Grant No. QP084401 via the Quantum Universe Center at Korea Institute for Advanced Study. The work of JK, SL, and JHS is supported by the National Research Foundation of Korea, Grant No. NRF-2019R1A2C1009419. C.T.L. is supported by KIAS Individual Grant No. PG075301

(C.T.L.).

-
- [1] ATLAS collaboration, G. Aad et al., *Observation of a new particle in the search for the Standard Model Higgs boson with the ATLAS detector at the LHC*, *Phys. Lett. B* **716** (2012) 1–29, [[1207.7214](#)].
 - [2] CMS collaboration, S. Chatrchyan et al., *Observation of a New Boson at a Mass of 125 GeV with the CMS Experiment at the LHC*, *Phys. Lett. B* **716** (2012) 30–61, [[1207.7235](#)].
 - [3] W. Buchmuller and D. Wyler, *Effective Lagrangian Analysis of New Interactions and Flavor Conservation*, *Nucl. Phys. B* **268** (1986) 621–653.
 - [4] G. C. Branco, P. M. Ferreira, L. Lavoura, M. N. Rebelo, M. Sher and J. P. Silva, *Theory and phenomenology of two-Higgs-doublet models*, *Phys. Rept.* **516** (2012) 1–102, [[1106.0034](#)].
 - [5] M. Aoki, S. Kanemura, K. Tsumura and K. Yagyu, *Models of Yukawa interaction in the two Higgs doublet model, and their collider phenomenology*, *Phys. Rev. D* **80** (2009) 015017, [[0902.4665](#)].
 - [6] M. Misiak and M. Steinhauser, *Weak radiative decays of the B meson and bounds on M_{H^\pm} in the Two-Higgs-Doublet Model*, *Eur. Phys. J. C* **77** (2017) 201, [[1702.04571](#)].
 - [7] ATLAS collaboration, M. Aaboud et al., *Search for charged Higgs bosons decaying via $H^\pm \rightarrow \tau^\pm \nu_\tau$ in the τ +jets and τ +lepton final states with 36 fb^{-1} of pp collision data recorded at $\sqrt{s} = 13 \text{ TeV}$ with the ATLAS experiment*, *JHEP* **09** (2018) 139, [[1807.07915](#)].
 - [8] CMS collaboration, A. M. Sirunyan et al., *Search for charged Higgs bosons in the $H^\pm \rightarrow \tau^\pm \nu_\tau$ decay channel in proton-proton collisions at $\sqrt{s} = 13 \text{ TeV}$* , *JHEP* **07** (2019) 142, [[1903.04560](#)].
 - [9] S. Abbaspour, S. M. Moosavi Nejad and M. Balali, *Indirect search for light charged Higgs bosons through the dominant semileptonic decays of top quark $t \rightarrow b(\rightarrow B/D + X) + H^\pm(\rightarrow \tau^\pm \nu_\tau)$* , *Nucl. Phys. B* **932** (2018) 505–528, [[1806.02546](#)].
 - [10] A. G. Akeroyd, S. Moretti and M. Song, *Light charged Higgs boson with dominant decay to quarks and its search at the LHC and future colliders*, *Phys. Rev. D* **98** (2018) 115024, [[1810.05403](#)].
 - [11] A. Arhrib, R. Benbrik, H. Harouiz, S. Moretti, Y. Wang and Q.-S. Yan, *Implications of a light charged Higgs boson at the LHC run III in the 2HDM*, *Phys. Rev. D* **102** (2020) 115040, [[2003.11108](#)].
 - [12] A. Arhrib, R. Benbrik and S. Moretti, *Bosonic Decays of Charged Higgs Bosons in a 2HDM Type-I*, *Eur. Phys. J. C* **77** (2017) 621, [[1607.02402](#)].
 - [13] G. K. Demir, N. Sönmez and H. Dogan, *Deep-Learning in Search of Light Charged Higgs*, [1803.01550](#).
 - [14] R. Dermisek, E. Lunghi and A. Raval, *Trilepton Signatures of Light Charged and CP-odd Higgs Bosons in Top Quark Decays*, *JHEP* **04** (2013) 063, [[1212.5021](#)].
 - [15] ATLAS collaboration, *Search for a light charged Higgs boson in $t \rightarrow H^\pm b$ decays, with $H^\pm \rightarrow cb$, in the lepton+jets final state in proton-proton collisions at $\sqrt{s} = 13 \text{ TeV}$ with the ATLAS detector*, .

- [16] ATLAS collaboration, G. Aad et al., *Search for a light charged Higgs boson in the decay channel $H^+ \rightarrow c\bar{s}$ in $t\bar{t}$ events using pp collisions at $\sqrt{s} = 7$ TeV with the ATLAS detector*, *Eur. Phys. J. C* **73** (2013) 2465, [[1302.3694](#)].
- [17] CMS collaboration, A. M. Sirunyan et al., *Search for a light charged Higgs boson decaying to a W boson and a CP -odd Higgs boson in final states with $e\mu\mu$ or $\mu\mu\mu$ in proton-proton collisions at $\sqrt{s} = 13$ TeV*, *Phys. Rev. Lett.* **123** (2019) 131802, [[1905.07453](#)].
- [18] CMS collaboration, A. M. Sirunyan et al., *Search for a charged Higgs boson decaying to charm and bottom quarks in proton-proton collisions at $\sqrt{s} = 8$ TeV*, *JHEP* **11** (2018) 115, [[1808.06575](#)].
- [19] CMS collaboration, V. Khachatryan et al., *Search for a light charged Higgs boson decaying to $c\bar{s}$ in pp collisions at $\sqrt{s} = 8$ TeV*, *JHEP* **12** (2015) 178, [[1510.04252](#)].
- [20] CMS collaboration, A. M. Sirunyan et al., *Search for a light charged Higgs boson in the $H^\pm \rightarrow cs$ channel in proton-proton collisions at $\sqrt{s} = 13$ TeV*, *Phys. Rev. D* **102** (2020) 072001, [[2005.08900](#)].
- [21] A. Arhrib, R. Benbrik, R. Enberg, W. Klemm, S. Moretti and S. Munir, *Identifying a light charged Higgs boson at the LHC Run II*, *Phys. Lett. B* **774** (2017) 591–598, [[1706.01964](#)].
- [22] S. Kanemura, K. Tsumura and H. Yokoya, *Multi-tau-lepton signatures at the LHC in the two Higgs doublet model*, *Phys. Rev. D* **85** (2012) 095001, [[1111.6089](#)].
- [23] A. Arhrib, R. Benbrik, M. Krab, B. Manaut, S. Moretti, Y. Wang et al., *New discovery modes for a light charged Higgs boson at the LHC*, *JHEP* **10** (2021) 073, [[2106.13656](#)].
- [24] A. Arhrib, R. Benbrik, M. Krab, B. Manaut, S. Moretti, Y. Wang et al., *New Light H^\pm Discovery Channels at the LHC*, *Symmetry* **13** (2021) 2319, [[2110.04823](#)].
- [25] S. Moretti and K. Odagiri, *Production of charged Higgs bosons of the minimal supersymmetric standard model in b quark initiated processes at the large hadron collider*, *Phys. Rev. D* **55** (1997) 5627–5635, [[hep-ph/9611374](#)].
- [26] J. Hernandez-Sanchez, S. Moretti, R. Noriega-Papaqui and A. Rosado, *Off-diagonal terms in Yukawa textures of the Type-III 2-Higgs doublet model and light charged Higgs boson phenomenology*, *JHEP* **07** (2013) 044, [[1212.6818](#)].
- [27] J. Hernández-Sánchez, C. G. Honorato, S. Moretti and S. Rosado-Navarro, *Charged Higgs boson production via cb -fusion at the Large Hadron Collider*, *Phys. Rev. D* **102** (2020) 055008, [[2003.06263](#)].
- [28] M. Aiko, S. Kanemura and K. Mawatari, *Exploring the global symmetry structure of the Higgs potential via same-sign pair production of charged Higgs bosons*, *Phys. Lett. B* **797** (2019) 134854, [[1906.09101](#)].
- [29] A. Arhrib, K. Cheung and C.-T. Lu, *Same-sign charged Higgs boson pair production in bosonic decay channels at the HL-LHC and HE-LHC*, *Phys. Rev. D* **102** (2020) 095026, [[1910.02571](#)].
- [30] O. Flores-Sánchez, J. Hernández-Sánchez, C. G. Honorato, S. Moretti and S. Rosado-Navarro, *Light charged Higgs boson production at the Large Hadron electron Collider*, *Phys. Rev. D* **99** (2019) 095009, [[1811.05476](#)].
- [31] A. G. Akeroyd, S. Moretti and M. Song, *Light charged Higgs boson with dominant decay to a*

- charm quark and a bottom quark and its search at LEP2 and future e^+e^- colliders, *Phys. Rev. D* **101** (2020) 035021, [[1908.00826](#)].
- [32] H. Bahl, T. Stefaniak and J. Wittbrodt, *The forgotten channels: charged Higgs boson decays to a W^\pm and a non-SM-like Higgs boson*, *JHEP* **06** (2021) 183, [[2103.07484](#)].
- [33] J. Song and Y. W. Yoon, *$W\gamma$ decay of the elusive charged Higgs boson in the two-Higgs-doublet model with vectorlike fermions*, *Phys. Rev. D* **100** (2019) 055006, [[1904.06521](#)].
- [34] S. Moretti and D. P. Roy, *Detecting heavy charged Higgs bosons at the LHC with triple b tagging*, *Phys. Lett. B* **470** (1999) 209–214, [[hep-ph/9909435](#)].
- [35] S. Moretti, R. Santos and P. Sharma, *Optimising Charged Higgs Boson Searches at the Large Hadron Collider Across $b\bar{b}W^\pm$ Final States*, *Phys. Lett. B* **760** (2016) 697–705, [[1604.04965](#)].
- [36] A. Arhrib, A. Jueid and S. Moretti, *Top quark polarization as a probe of charged Higgs bosons*, *Phys. Rev. D* **98** (2018) 115006, [[1807.11306](#)].
- [37] J. Bernon, J. F. Gunion, H. E. Haber, Y. Jiang and S. Kraml, *Scrutinizing the alignment limit in two-Higgs-doublet models. II. $m_H=125$ GeV*, *Phys. Rev. D* **93** (2016) 035027, [[1511.03682](#)].
- [38] S. Chang, S. K. Kang, J.-P. Lee and J. Song, *Higgs potential and hidden light Higgs scenario in two Higgs doublet models*, *Phys. Rev. D* **92** (2015) 075023, [[1507.03618](#)].
- [39] A. Jueid, J. Kim, S. Lee and J. Song, *Type-X two-Higgs-doublet model in light of the muon $g-2$: Confronting Higgs boson and collider data*, *Phys. Rev. D* **104** (2021) 095008, [[2104.10175](#)].
- [40] M. Carena, I. Low, N. R. Shah and C. E. M. Wagner, *Impersonating the Standard Model Higgs Boson: Alignment without Decoupling*, *JHEP* **04** (2014) 015, [[1310.2248](#)].
- [41] A. Celis, V. Ilisie and A. Pich, *LHC constraints on two-Higgs doublet models*, *JHEP* **07** (2013) 053, [[1302.4022](#)].
- [42] K. Cheung, J. S. Lee and P.-Y. Tseng, *Higgscision in the Two-Higgs Doublet Models*, *JHEP* **01** (2014) 085, [[1310.3937](#)].
- [43] J. Bernon, J. F. Gunion, H. E. Haber, Y. Jiang and S. Kraml, *Scrutinizing the alignment limit in two-Higgs-doublet models: $m_h=125$ GeV*, *Phys. Rev. D* **92** (2015) 075004, [[1507.00933](#)].
- [44] D. Das and I. Saha, *Search for a stable alignment limit in two-Higgs-doublet models*, *Phys. Rev. D* **91** (2015) 095024, [[1503.02135](#)].
- [45] S. Kanemura, Y. Okada, H. Taniguchi and K. Tsumura, *Indirect bounds on heavy scalar masses of the two-Higgs-doublet model in light of recent Higgs boson searches*, *Phys. Lett. B* **704** (2011) 303–307, [[1108.3297](#)].
- [46] N. Chen, T. Han, S. Li, S. Su, W. Su and Y. Wu, *Type-I 2HDM under the Higgs and Electroweak Precision Measurements*, *JHEP* **08** (2020) 131, [[1912.01431](#)].
- [47] S. L. Glashow and S. Weinberg, *Natural Conservation Laws for Neutral Currents*, *Phys. Rev. D* **15** (1977) 1958.
- [48] E. A. Paschos, *Diagonal Neutral Currents*, *Phys. Rev. D* **15** (1977) 1966.
- [49] D. Eriksson, J. Rathsmann and O. Stal, *2HDMC: Two-Higgs-Doublet Model Calculator Physics and Manual*, *Comput. Phys. Commun.* **181** (2010) 189–205, [[0902.0851](#)].
- [50] P. Bechtle, S. Heinemeyer, T. Klingl, T. Stefaniak, G. Weiglein and J. Wittbrodt, *HiggsSignals-2:*

- Probing new physics with precision Higgs measurements in the LHC 13 TeV era*, *Eur. Phys. J. C* **81** (2021) 145, [2012.09197].
- [51] P. Bechtle, D. Dercks, S. Heinemeyer, T. Klingl, T. Stefaniak, G. Weiglein et al., *HiggsBounds-5: Testing Higgs Sectors in the LHC 13 TeV Era*, *Eur. Phys. J. C* **80** (2020) 1211, [2006.06007].
 - [52] ATLAS collaboration, G. Aad et al., *Combined measurements of Higgs boson production and decay using up to 80 fb⁻¹ of proton-proton collision data at $\sqrt{s} = 13$ TeV collected with the ATLAS experiment*, *Phys. Rev. D* **101** (2020) 012002, [1909.02845].
 - [53] I. P. Ivanov, *Minkowski space structure of the Higgs potential in 2HDM*, *Phys. Rev. D* **75** (2007) 035001, [hep-ph/0609018].
 - [54] S. Kanemura, T. Kubota and E. Takasugi, *Lee-Quigg-Thacker bounds for Higgs boson masses in a two doublet model*, *Phys. Lett. B* **313** (1993) 155–160, [hep-ph/9303263].
 - [55] A. G. Akeroyd, A. Arhrib and E.-M. Naimi, *Note on tree level unitarity in the general two Higgs doublet model*, *Phys. Lett. B* **490** (2000) 119–124, [hep-ph/0006035].
 - [56] A. Barroso, P. M. Ferreira, I. P. Ivanov and R. Santos, *Metastability bounds on the two Higgs doublet model*, *JHEP* **06** (2013) 045, [1303.5098].
 - [57] H.-J. He, N. Polonsky and S.-f. Su, *Extra families, Higgs spectrum and oblique corrections*, *Phys. Rev. D* **64** (2001) 053004, [hep-ph/0102144].
 - [58] W. Grimus, L. Lavoura, O. M. Ogreid and P. Osland, *The Oblique parameters in multi-Higgs-doublet models*, *Nucl. Phys. B* **801** (2008) 81–96, [0802.4353].
 - [59] PARTICLE DATA GROUP collaboration, P. A. Zyla et al., *Review of Particle Physics*, *PTEP* **2020** (2020) 083C01.
 - [60] ATLAS collaboration, M. Aaboud et al., *Search for Higgs bosons produced via vector-boson fusion and decaying into bottom quark pairs in $\sqrt{s} = 13$ TeV pp collisions with the ATLAS detector*, *Phys. Rev. D* **98** (2018) 052003, [1807.08639].
 - [61] ATLAS collaboration, M. Aaboud et al., *Measurements of gluon-gluon fusion and vector-boson fusion Higgs boson production cross-sections in the $H \rightarrow WW^* \rightarrow e\nu\mu\nu$ decay channel in pp collisions at $\sqrt{s} = 13$ TeV with the ATLAS detector*, *Phys. Lett. B* **789** (2019) 508–529, [1808.09054].
 - [62] ATLAS collaboration, M. Aaboud et al., *Cross-section measurements of the Higgs boson decaying into a pair of τ -leptons in proton-proton collisions at $\sqrt{s} = 13$ TeV with the ATLAS detector*, *Phys. Rev. D* **99** (2019) 072001, [1811.08856].
 - [63] ATLAS collaboration, G. Aad et al., *Higgs boson production cross-section measurements and their EFT interpretation in the 4ℓ decay channel at $\sqrt{s} = 13$ TeV with the ATLAS detector*, *Eur. Phys. J. C* **80** (2020) 957, [2004.03447].
 - [64] CMS collaboration, A. M. Sirunyan et al., *Search for $t\bar{t}H$ production in the $H \rightarrow b\bar{b}$ decay channel with leptonic $t\bar{t}$ decays in proton-proton collisions at $\sqrt{s} = 13$ TeV*, *JHEP* **03** (2019) 026, [1804.03682].
 - [65] CMS collaboration, A. M. Sirunyan et al., *Search for the Higgs boson decaying to two muons in proton-proton collisions at $\sqrt{s} = 13$ TeV*, *Phys. Rev. Lett.* **122** (2019) 021801, [1807.06325].
 - [66] CMS collaboration, *Measurements of properties of the Higgs boson in the four-lepton final state*

in proton-proton collisions at $\sqrt{s} = 13$ TeV, .

- [67] CMS collaboration, *Measurements of differential Higgs boson production cross sections in the leptonic WW decay mode at $\sqrt{s} = 13$ TeV, .*
- [68] CMS collaboration, A. M. Sirunyan et al., *Measurements of the Higgs boson width and anomalous HVV couplings from on-shell and off-shell production in the four-lepton final state*, *Phys. Rev. D* **99** (2019) 112003, [[1901.00174](#)].
- [69] ATLAS collaboration, M. Aaboud et al., *Search for Higgs boson decays into a pair of light bosons in the $b\bar{b}\mu\mu$ final state in pp collision at $\sqrt{s} = 13$ TeV with the ATLAS detector*, *Phys. Lett. B* **790** (2019) 1–21, [[1807.00539](#)].
- [70] ATLAS collaboration, M. Aaboud et al., *Search for the Higgs boson produced in association with a vector boson and decaying into two spin-zero particles in the $H \rightarrow aa \rightarrow 4b$ channel in pp collisions at $\sqrt{s} = 13$ TeV with the ATLAS detector*, *JHEP* **10** (2018) 031, [[1806.07355](#)].
- [71] CMS collaboration, A. M. Sirunyan et al., *Search for an exotic decay of the Higgs boson to a pair of light pseudoscalars in the final state of two muons and two τ leptons in proton-proton collisions at $\sqrt{s} = 13$ TeV*, *JHEP* **11** (2018) 018, [[1805.04865](#)].
- [72] CMS collaboration, A. M. Sirunyan et al., *Search for an exotic decay of the Higgs boson to a pair of light pseudoscalars in the final state with two muons and two b quarks in pp collisions at 13 TeV*, *Phys. Lett. B* **795** (2019) 398–423, [[1812.06359](#)].
- [73] CMS collaboration, A. M. Sirunyan et al., *Search for an exotic decay of the Higgs boson to a pair of light pseudoscalars in the final state with two b quarks and two τ leptons in proton-proton collisions at $\sqrt{s} = 13$ TeV*, *Phys. Lett. B* **785** (2018) 462, [[1805.10191](#)].
- [74] CMS collaboration, A. M. Sirunyan et al., *Search for light pseudoscalar boson pairs produced from decays of the 125 GeV Higgs boson in final states with two muons and two nearby tracks in pp collisions at $\sqrt{s} = 13$ TeV*, *Phys. Lett. B* **800** (2020) 135087, [[1907.07235](#)].
- [75] E. Braaten and J. P. Leveille, *Higgs Boson Decay and the Running Mass*, *Phys. Rev. D* **22** (1980) 715.
- [76] M. Drees and K.-i. Hikasa, *NOTE ON QCD CORRECTIONS TO HADRONIC HIGGS DECAY*, *Phys. Lett. B* **240** (1990) 455.
- [77] S. G. Gorishnii, A. L. Kataev, S. A. Larin and L. R. Surguladze, *Corrected Three Loop QCD Correction to the Correlator of the Quark Scalar Currents and γ (Tot) ($H^0 \rightarrow$ Hadrons)*, *Mod. Phys. Lett. A* **5** (1990) 2703–2712.
- [78] J. Alwall, R. Frederix, S. Frixione, V. Hirschi, F. Maltoni, O. Mattelaer et al., *The automated computation of tree-level and next-to-leading order differential cross sections, and their matching to parton shower simulations*, *JHEP* **07** (2014) 079, [[1405.0301](#)].
- [79] NNPDF collaboration, R. D. Ball et al., *Parton distributions from high-precision collider data*, *Eur. Phys. J. C* **77** (2017) 663, [[1706.00428](#)].
- [80] D. Gonçalves, T. Han, F. Kling, T. Plehn and M. Takeuchi, *Higgs boson pair production at future hadron colliders: From kinematics to dynamics*, *Phys. Rev. D* **97** (2018) 113004, [[1802.04319](#)].
- [81] C. Degrande, C. Duhr, B. Fuks, D. Grellscheid, O. Mattelaer and T. Reiter, *UFO - The Universal*

- FeynRules Output*, *Comput. Phys. Commun.* **183** (2012) 1201–1214, [[1108.2040](#)].
- [82] T. Sjostrand, S. Mrenna and P. Z. Skands, *A Brief Introduction to PYTHIA 8.1*, *Comput. Phys. Commun.* **178** (2008) 852–867, [[0710.3820](#)].
 - [83] DELPHES 3 collaboration, J. de Favereau, C. Delaere, P. Demin, A. Giammanco, V. Lemaître, A. Mertens et al., *DELPHES 3, A modular framework for fast simulation of a generic collider experiment*, *JHEP* **02** (2014) 057, [[1307.6346](#)].
 - [84] M. Cacciari, G. P. Salam and G. Soyez, *FastJet User Manual*, *Eur. Phys. J. C* **72** (2012) 1896, [[1111.6097](#)].
 - [85] CMS collaboration, A. M. Sirunyan et al., *Performance of reconstruction and identification of τ leptons decaying to hadrons and ν_τ in pp collisions at $\sqrt{s} = 13$ TeV*, *JINST* **13** (2018) P10005, [[1809.02816](#)].
 - [86] ATLAS collaboration, *Measurement of the tau lepton reconstruction and identification performance in the ATLAS experiment using pp collisions at $\sqrt{s} = 13$ TeV*, .
 - [87] M. Cacciari and G. P. Salam, *Pileup subtraction using jet areas*, *Phys. Lett. B* **659** (2008) 119–126, [[0707.1378](#)].
 - [88] ATLAS collaboration, *Expected performance for an upgraded ATLAS detector at High-Luminosity LHC*, .
 - [89] ATLAS collaboration, *Study of the double Higgs production channel $H(\rightarrow b\bar{b})H(\rightarrow \gamma\gamma)$ with the ATLAS experiment at the HL-LHC*, .
 - [90] G. Cowan, K. Cranmer, E. Gross and O. Vitells, *Asymptotic formulae for likelihood-based tests of new physics*, *Eur. Phys. J. C* **71** (2011) 1554, [[1007.1727](#)].
 - [91] M. L. Mangano, M. Moretti, F. Piccinini and M. Treccani, *Matching matrix elements and shower evolution for top-quark production in hadronic collisions*, *JHEP* **01** (2007) 013, [[hep-ph/0611129](#)].